# Sol-Gel Auto-Combustion Synthesis and Luminescence Properties of GdCaAl3O7:RE3+ (RE=Eu, Tb, Eu@Tb) Phosphors For Near-Ultraviolet Light-Triggered Indoor Illumination

**Haoran Zhou**
Ningbo University

**Xin Chen**
Ningbo University

**L.W. Jiang** ( jianglinwen@nbu.edu.cn )
Ningbo University https://orcid.org/0000-0002-8264-0102

**Anhua Wu**
Shanghai Institute of Ceramics Chinese Academy of Sciences

**Laihui Luo**
Ningbo University

**Hongbing Chen**
Ningbo University

**Research Article**

**Keywords:** Sol-gel, Auto-combustion, GdCaAl3O7, Phosphors, Luminescence properties

**Posted Date:** May 20th, 2021

**DOI:** https://doi.org/10.21203/rs.3.rs-520201/v1



**Version of Record:** A version of this preprint was published at Journal of Luminescence on February 1st, 2022. See the published version at https://doi.org/10.1016/j.jlumin.2022.118774.

# Sol-gel auto-combustion synthesis and luminescence properties of $GdCaAl_3O_7$: $RE^{3+}$ (RE=Eu, Tb, Eu@Tb) phosphors for near-ultraviolet light-triggered indoor illumination

Haoran ZHOU[a,1], Xin CHEN[a,1], Linwen JIANG[a*], Anhua WU[b], Laihui LUO[c], Hongbing CHEN[a]

[a]State Key Laboratory Base of Novel Functional Materials and Preparation Science, Key Laboratory of Photoelectric Detection Materials and Devices of Zhejiang Province, Ningbo University, Ningbo 315211, P. R. China

[b]Shanghai Institute of Ceramics, Chinese Academy of Sciences, Shanghai 201800, P. R. China

[c]Department of Microelectronic Science and Engineering, School of Physical Science and Technology, Ningbo University, Ningbo 315211, P. R. China

## Abstract

The color-tunable $GdCaAl_3O_7$: $RE^{3+}$ (RE=Eu, Tb, Eu@Tb) phosphors were synthesized via an ultrafast sol-gel auto-combustion synthesis method. The XRD (X-ray diffraction) patterns confirmed the forming of $GdCaAl_3O_7$ tetragonal phase, and the SEM (Scanning electron microscopy) images indicated that the obtained products presented honeycomb-like structure due to the gas releasing during the auto-combustion process. The EDS (Energy dispersion spectra) results suggest that $Eu^{3+}$ and $Tb^{3+}$ were well incorporated into the host matrices of $GdCaAl_3O_7$. The luminescent properties, concentration quenching mechanism, energy transfer mechanism, luminescent dynamics, thermal stability and product practicability of $GdCaAl_3O_7$: $R^{3+}$ (RE=Eu, Tb, Eu@Tb) phosphors were investigated systematically. All the $GdCaAl_3O_7$: $RE^{3+}$ (RE=Eu, Tb, Eu@Tb) products presented the characteristic emission of doped $RE^{3+}$. Using $GdCaAl_3O_7$: 50% $Tb^{3+}$@3.0% $Eu^{3+}$ as yellow-emitting phosphors in combination with commercial BAM: $Eu^{2+}$ blue-emitting phosphors and a NUV chip can successfully package a warm white LED device with high color rendering index (CRI, 86.3) and low correlated color temperature (CCT, 3348 K) that was very suitable for near-ultraviolet light-triggered indoor illumination.

**Key words:** Sol-gel; Auto-combustion; $GdCaAl_3O_7$; Phosphors; Luminescence properties;

## 1. Introduction

With the enhancing of people's awareness for protecting the environment, the studying of phosphor-converted white light emitting diodes (pc-WLEDs) had attracted much attention due to the eminent advantages in high luminescent efficiency, low energy consumption, superior lifetime and excellent reliability. The pc-WLEDs as eco-benign products have become the most potential light

*Corresponding author.
*E-mail address:* jianglinwen@nbu.edu.cn (Linwen Jiang).

source in the next generation [1-10]. Moreover, trivalent rare-earth ions ($RE^{3+}$)-doped aluminate phosphors are appropriate for light-conversion materials owing to their excellent luminescent efficiency, high chemical and thermal stability [5,7,8,11-14].

Among them, $GdCaAl_3O_7$ can be employed as an efficient luminescent host because of their outstanding optical damage threshold and high ultraviolet (UV) absorption, which was considered as one of the best phosphor candidates in pc-WLEDs [15,16]. In addition, $GdCaAl_3O_7$ belongs to the aluminate-based melilite family with the compound formula of $ABC_3O_7$ (A= Ca, Sr, Ba; B=Y, La, Gd; C=Al, Ga). These melilite compounds form tetragonal crystals belonging to the space group $P\text{-}42_1m$, containing five-membered rings constituted from $AlO_4^{5-}$ tetrahedral in which $A^{2+}$ ions and $B^{3+}$ ions are distributed randomly at the eight-coordinated sites with $C_s$ symmetry, while $Al^{3+}$ ions occupy two non-equivalent tetragonal sites with both $S_4$ and $C_s$ symmetries [17-21].

Excellent phosphors not only require suitable host matrix but also appropriate activated ions as emission source. $RE^{3+}$-activated inorganic phosphors are stable and can present strong emission properties owing to the well-known 4f intra-configurational electronic transitions under the UV or near-UV (NUV) irradiation, especially $Eu^{3+}$ and $Tb^{3+}$ [6,8,11,22-26]. Since the electrons are well shielded from neighboring ions so sharp and discrete energy levels can be obtained in $RE^{3+}$ [27-30]. According to the present literatures, the respective luminescent properties of $Eu^{3+}$ and $Tb^{3+}$ played an important role in the application of pc-WLEDs and had attracted a lot of attention by researchers in the recent years. For example, U. Farooq et al. suggested that the $Na_{3.6}Y_{1.8}(PO_4)_3$: $Eu^{3+}$ could be used as red-emitting phosphors for a WLED device via combining the commercial phosphors [31], X. Huang et al. demonstrated that the $Ba_3Lu_2B_6O_{15}$:$Ce^{3+}$,$Tb^{3+}$ phosphors could emit white light with high color rendering index pumped by NUV chip, and M. Song et al. reported the $KBaGd(WO_4)_3$ phosphors for white light emission by suitably controlling the doping ratios of $Eu^{3+}$ and $Tb^{3+}$ [5,24].The above results suggest that $Eu^{3+}$ and $Tb^{3+}$ activated phosphors are excellent candidates for solid-sate lighting.

In general, phosphors can be prepared by many synthesis methods including sol-gel, hydrothermal synthesis, microwave heating, solid-state reaction and solution combustion [16,19,20,32,33]. The main disadvantages of the traditional solid-state method include high reaction temperature, large particle sizes and inhomogeneous mixing [16,18,21,34]. The sol–gel auto-combustion synthesis is a suitable method in preparing multi-component oxides owing to the

high reaction rate at a relatively low ignition temperature. Furthermore, the experimental process is easy to manipulate and the total experimental period is short. It is very beneficial to prepare the multi-component oxides with uniform size and high purity [13,19,20]. In this work, we employed this sol-gel auto-combustion method for fabricating $GdCaAl_3O_7$: $RE^{3+}$ (RE=Eu, Tb, Eu@Tb) phosphors. The occupation and the interaction of lattice sites between the doped $Eu^{3+}$ and $Tb^{3+}$ were discussed based on the crystal structure. The luminescent properties and energy transfer of $Eu^{3+}$ and $Tb^{3+}$ in $GdCaAl_3O_7$ were investigated. The results show that the emission color of the phosphors could be tuned continuously from green to yellow and red by changing the ratio of $Eu^{3+}/Tb^{3+}$. Finally, warm white-emitting devices were fabricated by utilizing the optimal co-doped products and $BaMgAl_{10}O_{17}$: $Eu^{2+}$ for covering NUV chips.

## 2. Experimental process

### 2.1 Chemicals and reagents

All the starting chemicals and reagents in the experiments without further purification, including $Al(NO_3)_3 \cdot 9H_2O$ (A. R. 99.9%), $CaCO_3$ (A. R. 99.9%), $Gd_2O_3$ (99.99%), $Eu_2O_3$ (99.99%), $Tb_2O_3$ (99.99%) and $C_2H_5NO_2$ (A. R. 99.9%) were purchased from the Aladdin Chemical Reagent Company.

### 2.2 Synthesis of $GdCaAl_3O_7$: $Eu^{3+}$@$Tb^{3+}$ phosphors

A series of $GdCaAl_3O_7$: $RE^{3+}$ (RE=Eu, Tb, Eu@Tb) phosphors were prepared by a sol-gel auto-combustion synthesis method. The chemical equation for the reaction is [19]:

$$(1-\mathrm{x}-\mathrm{y})Gd_2O_3 + xEu_2O_3 + yTb_2O_3 + 2CaCO_3 + HNO_3 + 6Al(NO_3)_3 + 5C_2H_5NO_2 \rightarrow$$
$$2Gd_{1-x-y}Eu_xTb_yCaAl_3O_7 + Gas\uparrow.$$

In a representative synthesis process, solution A was prepared by dissolving the stoichiometric amounts of $Gd_2O_3$, $Eu_2O_3$ and $Tb_2O_3$ in about 6 mL nitric acid and mixed with the solution B which was prepared by dissolving the stoichiometric amounts of ingredients ($Al(NO_3)_3 \cdot 9H_2O$, $CaCO_3$) in distilled water. Meanwhile, the $C_2H_5NO_2$ was added to above solution to obtain a homogeneous aqueous solution (the mole amount of glycine was equal to the total mole amount of metal ions). Subsequently, the mixed aqueous solution was stirred continuously under the heating temperature of 70°C until the sticky gels were formed. The obtained gels were shifted into an open alumina crucible for the next the combustion experiments. The gels were burnt by a self-propagating combustion

manner at a relatively low ignition temperature. Initially, the solutions were dehydrated rapidly along with the gas volatilization. Subsequently, the dehydrated gels were ignited following by lots of brown fumes ($CO_2$, $N_2$, $NO_x$ and $H_2O$) [35]. Finally, a mass of porous products were obtained, while the as-prepared products presented brown owing to the residual organic matters. The as-prepared products were heated at different temperatures for 2 h in order to eliminate the unreacted matters and form single-phase $Gd_{1-x}Eu_xTb_yCaAl_3O_7$ phosphors. **Fig. 1** shows the flowchart of fabricating $GdCaAl_3O_7$**:** $Eu^{3+}$@$Tb^{3+}$ phosphors by the sol-gel auto-combustion method using glycine as combustion agent.

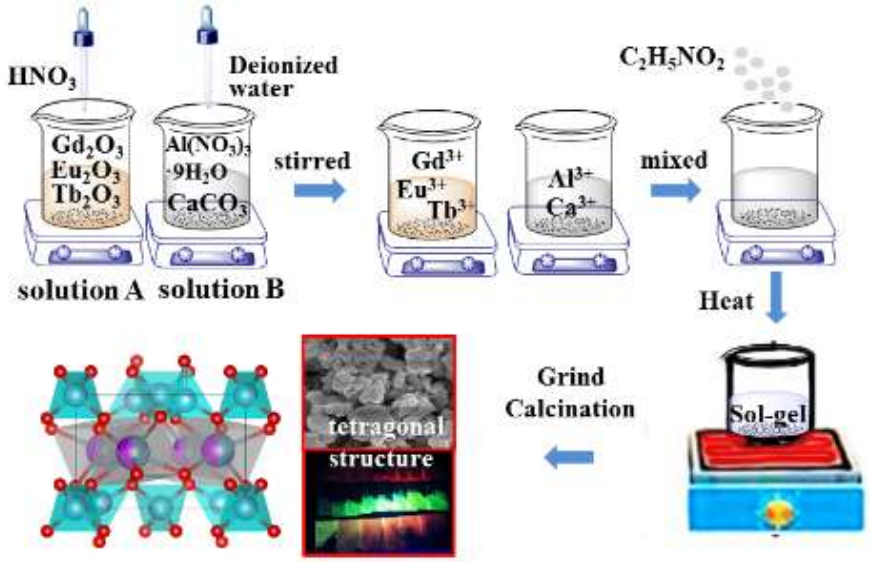


**Fig. 1** Schematic illustration of synthesis of $GdCaAl_3O_7$ phosphors doped with $Eu^{3+}$ and $Tb^{3+}$.

### 2.3 Phase structure, morphology and luminescence characterizations

The components of all the samples were clarified using an X-ray diffraction (XRD, Bruker D8 Advance) with Cu Ka radiation (λ= 1.54051 Å). The morphology and elemental composition were analyzed by utilizing a field-emission scanning electron microscope (FE-SEM; HITACHI SU3500) with an attached energy dispersive spectrometer (EDS). The luminescence spectra and decay curves were recorded by means of an Edinburgh FS5 fluorescence spectrometer using a pulsed xenon lamp as excitation source. The surrounding temperature of samples in the range of 183-423 K was adjusted by the temperature-controlled system (Linkam HFS600EPB2).

### 2.4 Fabrication of NUV chip-based white-LED devices

The NUV chip-based white-LED lamps were fabricated by combining the commercial $BaMgAl_{10}O_{17}:Eu^{2+}$ (BAM: $Eu^{2+}$) blue phosphors and the obtained $GdCaAl_3O_7$: 3.0% $Eu^{3+}$@50%

$Tb^{3+}$ phosphors with epoxy resin, and then coated on the surface of the commercial NUV (B365 nm) chip. After heating at 80 °C for 2 h, the NUV chip-based white-LED lamp was obtained. The photoelectric properties, such as electroluminescence (EL) emission spectra, color rendering index (CRI), correlated color temperature (CCT), color coordinates and luminous efficiency were recorded by using a multi-channel spectroradiometer system (MEASUREFINE; SPEC-3000A) attached with an integrating sphere.

## 3. Results and discussion

### 3.1 Structural and morphological analysis

The phase structures of samples were determined by XRD method. **Fig. 2a** indicates the XRD patterns of $GdCaAl_3O_7$ samples annealed at various temperatures. The results show that the XRD patterns of samples were in good agreement with the standard JCPDS card of $GdCaAl_3O_7$ (No. 50-1807) and the diffraction peak intensity enhanced with increasing the annealing temperatures, suggesting that pure $GdCaAl_3O_7$ can be obtained above the annealing temperature of 800 °C. The XRD patterns of doped $GdCaAl_3O_7$ samples including $GdCaAl_3O_7$: 40% $Eu^{3+}$, $GdCaAl_3O_7$: 50% $Tb^{3+}$ and $GdCaAl_3O_7$: 50% $Tb^{3+}$ @3.0% $Eu^{3+}$ were shown in **Fig. 2b**. It can be seen that all the major diffraction peaks were exactly matched with the standard JCPDS card. Therefore, it is reasonable to believe that the pure $GdCaAl_3O_7$ phase was retained when $RE^{3+}$ ions were doped into the $GdCaAl_3O_7$ host materials. Due to the similar electrovalence and cation radius, it could be known that the $Gd^{3+}$ ions could be well replaced by other $RE^{3+}$ ions in $GdCaAl_3O_7$ host lattices. Generally, the radius percentage difference ($D_r$) can be employed to evaluate the possibilities of forming a new solid solution, which can be expressed as below [36]:

$$D_r = \frac{R_1(CN) - R_2(CN)}{R_1(CN)} \times 100\% \quad (1)$$

In this formula, $R_1(CN)$ represents the radius of the replaced ions, and $R_2(CN)$ stands for the radius of dopant. In the case of the coordinate number 6, the radii of $Gd^{3+}$, $Eu^{3+}$ and $Tb^{3+}$ were 1.053, 1.066 and 1.04 Å, respectively. Accordingly, all the $D_r$ of doped $GdCaAl_3O_7$ were calculated as approximately 1.2 %, much lower than required 15%. It is well consistent with the formation rule of substitution-type solid solution proposed by Davolos [37], further indicating the feasibility of fabricating the $RE^{3+}$-doped $GdCaAl_3O_7$. In order to know clearly the crystal configuration and surrounding environment of the $GdCaAl_3O_7$ host lattices, a unit cell of $GdCaAl_3O_7$ crystal structure

was given. The corresponding cell parameters of $GdCaAl_3O_7$ were a = b = 7.801 Å, c = 5.132 Å and α = β = γ = 90°, as shown in **Fig. 2c**. In $GdCaAl_3O_7$, the frames of crystal structure are consisted of five-membered rings by linked tetrahedral $AlO_4^{5-}$ at each corner. As reported, $Al^{3+}$ ions were coordinated with four surrounding $O^{2-}$, and formed tetragonal structures. The $Ca^{2+}$ and $Gd^{3+}$ are randomly distributed at the centers of these rings which were in the octahedral coordination surrounded by six oxygen ions [15-18].

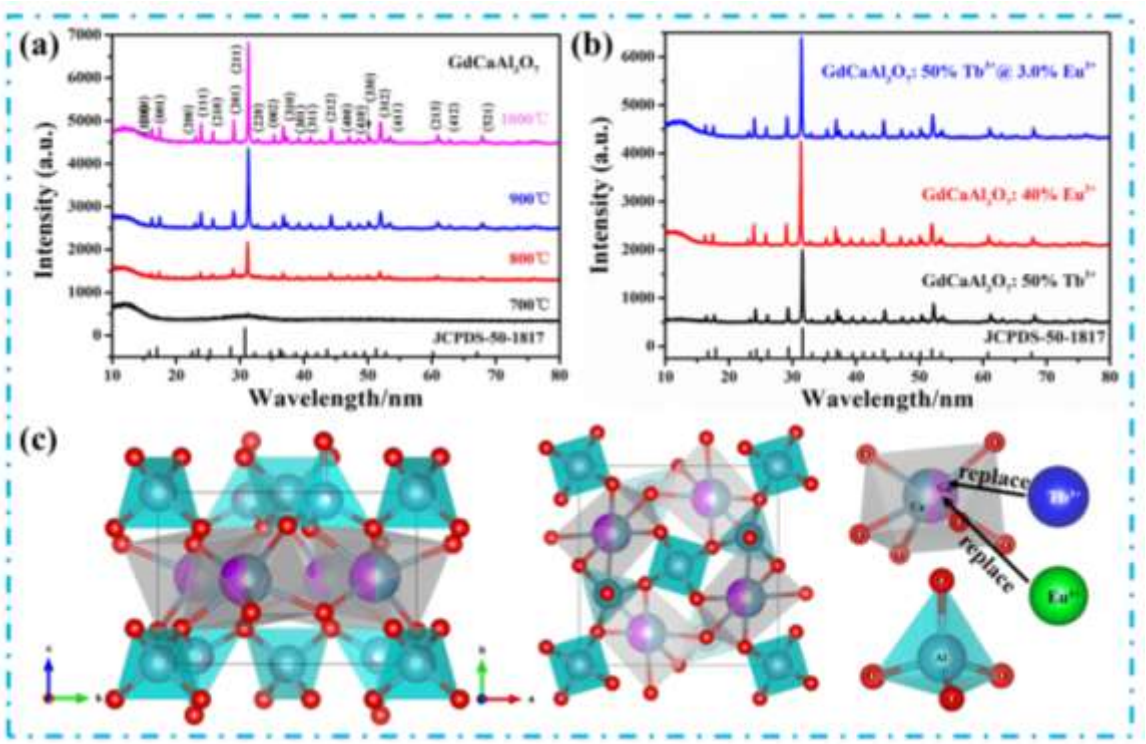


**Figure 2.** (a) XRD patterns of pure $GdCaAl_3O_7$ annealed at various temperatures. (b) XRD patterns of $GdCaAl_3O_7$: 50% $Tb^{3+}$, $GdCaAl_3O_7$: 40% $Eu^{3+}$ and $GdCaAl_3O_7$: 50% $Tb^{3+}$@3.0% $Eu^{3+}$ samples annealed at 1000 °C. (c) Crystal structure of $GdCaAl_3O_7$ unit cell (wherein $Ca^{2+}$ and $Gd^{3+}$ are located in octahedral; $Al^{3+}$ are located in tetrahedral; $O^{2-}$ are as coordinated ions; $Eu^{3+}$ and $Tb^{3+}$ ions substituted for $Gd^{3+}$ on octahedral sites).

The lattice constants and cell volumes of prepared $GdCaAl_3O_7$ samples were investigated by Jade analysis software using the XRD data, as shown in **Table 1**. It can be known that the lattice constants (a b c) of $GdCaAl_3O_7$ increased slightly as the annealing temperatures increased, and became close with the standard $GdCaAl_3O_7$. The grain sizes can be calculated by Scherrer's equation [38]:

$$D = 0.89\lambda/\beta cos\theta \quad (2)$$

Where $\lambda$ represents the X-ray wavelength ($\lambda$= 1.541 Å), $\theta$ stands for the diffraction angle, and $\beta$ corresponds to the half-height width of diffraction peak at $2\theta$. The grain sizes of $GdCaAl_3O_7$ exhibited an obvious increasing from 35 nm to 50 nm in the temperature range of 800-1000 °C.

**Table 1** The comparison of lattice parameters of $GdCaAl_3O_7$ samples at various annealing temperatures.

| Lattice parameters | Standard $GdCaAl_3O_7$ | Pure $GdCaAl_3O_7$ | | |
|---|---|---|---|---|
| | | 1000℃ | 900℃ | 800℃ |
| a (Å) | 7.8013 | 7.79819 | 7.77009 | 7.75826 |
| b (Å) | 7.8013 | 7.79819 | 7.77009 | 7.75826 |
| c (Å) | 5.1321 | 5.1301 | 5.15707 | 5.16586 |
| α (°) | 90 | 90 | 90 | 90 |
| β (°) | 90 | 90 | 90 | 90 |
| γ (°) | 90 | 90 | 90 | 90 |
| V (Å$^3$) | 312.3 | 311.97 | 311.35 | 310.94 |

**Fig. 3a** shows the EDS spectra and elemental mapping images of $GdCaAl_3O_7$: 50% $Tb^{3+}$@3.0% $Eu^{3+}$ samples. In **Fig. 3a**, it is clear that all the elements of Gd, Ca, Al, Eu and Tb were well distributed in the samples. Meanwhile, the EDS results show that the molar ratio of $Gd^{3+}$, $Al^{3+}$, $Eu^{3+}$ and $Tb^{3+}$ is equal to 1: 3.20: 0.032: 0.50, as shown in the inset table of **Fig. 3a**. This result is very close with the theoretical stoichiometric ratio of 1: 3: 0.03: 0.50, further suggesting that $Eu^{3+}$ and $Tb^{3+}$ were well doped into the host lattices. An obvious Pt peak at around 2.3 keV was observed in the EDS spectra since the Pt was employed as a measurement electrode [39]. The SEM images of $GdCaAl_3O_7$: 50% $Tb^{3+}$@3.0% $Eu^{3+}$ samples at different magnifications are shown in **Fig. 3b-d**. The obtained products have honeycomb-like structure with plenty of irregular pores because of the gas releasing during the process of sol-gel combustion reaction. The particle sizes were dispersed from 50-300 nm. Totally speaking, the product microstructure displayed the features of cross linking and compact bonding.

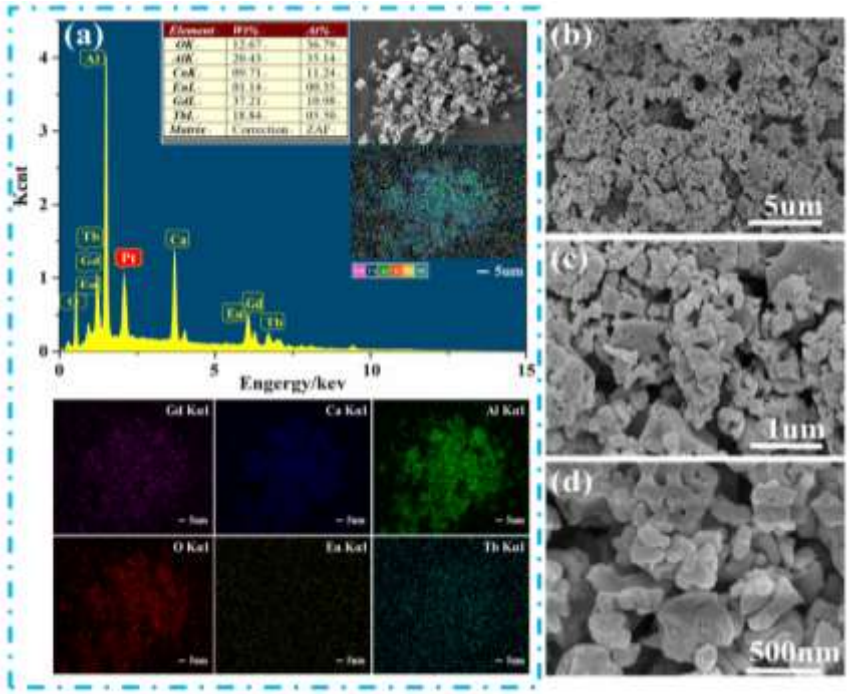


**Fig. 3** (a) EDS spectral patterns and elemental mapping images, (b-d) SEM images of $GdCaAl_3O_7$: 50% $Tb^{3+}$@3.0% $Eu^{3+}$ samples annealed at 1000 °C.

### 3.2 Luminescent properties of $GdCaAl_3O_7$: x% $Eu^{3+}$

To investigate the luminescent properties of the obtained products, the representative photoluminescence (PL) excitation and emission spectra of the $GdCaAl_3O_7$: 10% $Eu^{3+}$ are exhibited in **Fig. 4a**. It can be seen that the excitation spectra were consisted of several main absorption peaks at about 316 nm ($^7F_0 \rightarrow {}^5H_J$), 362 nm ($^7F_0 \rightarrow {}^5D_4$), 382 nm ($^7F_0 \rightarrow {}^5L_7$), 393 nm ($^7F_0 \rightarrow {}^5L_6$), 413 nm ($^7F_0 \rightarrow {}^5D_3$) and 463 nm ($^7F_0 \rightarrow {}^5D_2$) by monitoring 617 nm emission. Meanwhile, it can be observed that there are some intense peaks in the emission spectra at about 579, 587, 617, 655 and 702 nm under 393 nm excitation, which are associated with the transitions from $^5D_0$ to $^7F_j$ (j=0, 1, 2, 3, 4), respectively, originating from the intra 4f-4f electronic transitions of $Eu^{3+}$. Generally, the characteristic transition ($^5D_0 \rightarrow {}^7F_2$) of $Eu^{3+}$ as a main emission peak is related to the electronic dipole transition, and exhibited a intense peak at around 617 nm excitation in phosphors, such as $SrAl_2Si_2O_8$: $Eu^{3+}$ and $Y_2Mg_2Al_2Si_2O_{12}$: $Eu^{3+}$ phosphors [40,41]. The PL emission spectra for different $Eu^{3+}$ concentrations were depicted in **Fig. 4b**, which are very similar with those in the **Fig. 4a**. On the other hand, it can be easily found that the $Eu^{3+}$ concentrations had a great impact on the luminescent intensity of the $GdCaAl_3O_7$: x% $Eu^{3+}$. The emission intensity enhanced obviously with increasing the $Eu^{3+}$ concentrations until x = 40, and then decreased due to the well-known concentration quenching

effects induced by non-radiative (NR) energy transfer among the neighboring $Eu^{3+}$, suggesting that the optimal concentration of $Eu^{3+}$ was 40% in $GdCaAl_3O_7$: x% $Eu^{3+}$. The integrated emission intensity under various $Eu^{3+}$ concentrations was shown in **Fig. 4c**. It is necessary to study in detail the involved interaction about concentration quenching. Generally, the electric multipolar interaction and radiation reabsorption leaded to the NR energy transfer processes. Nevertheless, we cannot find any overlaps from the emission spectra, suggesting that the electric multipolar interaction would be more possible to generate the NR energy transfer processes and leaded to the concentration quenching rather than the radiation reabsorption [33]. The below Eq. (3) given by Dexter theory can be used to explain the mechanism of concentration quenching [10]:

$$\frac{I}{x} = k(1 + \beta(x)^{Q/3})^{-1} \quad (3)$$

Here, $I$ and $x$ stand for the emission intensity and doping concentration, respectively. $k$ and $\beta$ are coefficients dependent on $I$ and $x$. As we know, the electric multipolar owns three kinds of distinct interactions, and the $Q$ value represents the basic reasons of concentration quenching, wherein $Q$= 6, 8, and 10 correspond to dipole-dipole, dipole-quadrupole and quadrupole- quadrupole interactions, respectively. The inset in **Fig. 4c** displays the relation between the $log(x)$ and $log(I/x)$, and the experimental data were well matched to a straight line with a slope of -2.09, which means that the $Q$ value was estimated as about 6, indicating that the dipole-dipole interaction was the most possible to control the concentration quenching in $GdCaAl_3O_7$: x% $Eu^{3+}$.

The luminescence results in $GdCaAl_3O_7$: x% $Eu^{3+}$ can be explained by the luminescence energy transfer mechanism. The schematic diagram of energy transfer mechanism of $Eu^{3+}$ is presented in **Fig. 4d**. Under 393 nm excitation, the $Eu^{3+}$ in the $^7F_0$ ground state can absorb pump photons and transfer to excited level of $^5D_2$, $^5D_3$, $^5L_6$, $^5L_7$ and $^5D_4$. The excited $Eu^{3+}$ jumped into the $^5D_0$ level via the non-radiative process route dominated by the dipole-dipole interaction. Eventually, the excited $^5D_0$ state decayed to the $^7F_0$, $^7F_1$, $^7F_2$, $^7F_3$ and $^7F_4$ states by radiative multiphoton relaxation steps, following the characteristic emissions of $Eu^{3+}$ centered at 578, 588, 617, 656 and 702 nm, respectively. To visualize clearly the alteration of emission color, the Commission Internationale de I'Eclairage (CIE) chromaticity coordinates of the $GdCaAl_3O_7$: x% $Eu^{3+}$ phosphors are calculated according to emission intensity. It can be seen from **Fig. 4e** that the CIE chromaticity coordinate of the $GdCaAl_3O_7$: x% $Eu^{3+}$ changed from (0.6456, 0.3537) to (0.647, 0.3524), and then the red light

got deeper with increasing $Eu^{3+}$ contents. The optimal red color could be acquired when the doping content of $Eu^{3+}$ was up to 40%. The photographs of $GdCaAl_3O_7$: x% $Eu^{3+}$ phosphors under 365 nm UV-lamp are presented in the inset of **Fig. 4e**. It can be seen that the emission color of phosphors changed gradually, suggesting that the $GdCaAl_3O_7$: x% $Eu^{3+}$ can be employed as a kind of good red-emitting phosphors for solid-state lighting.

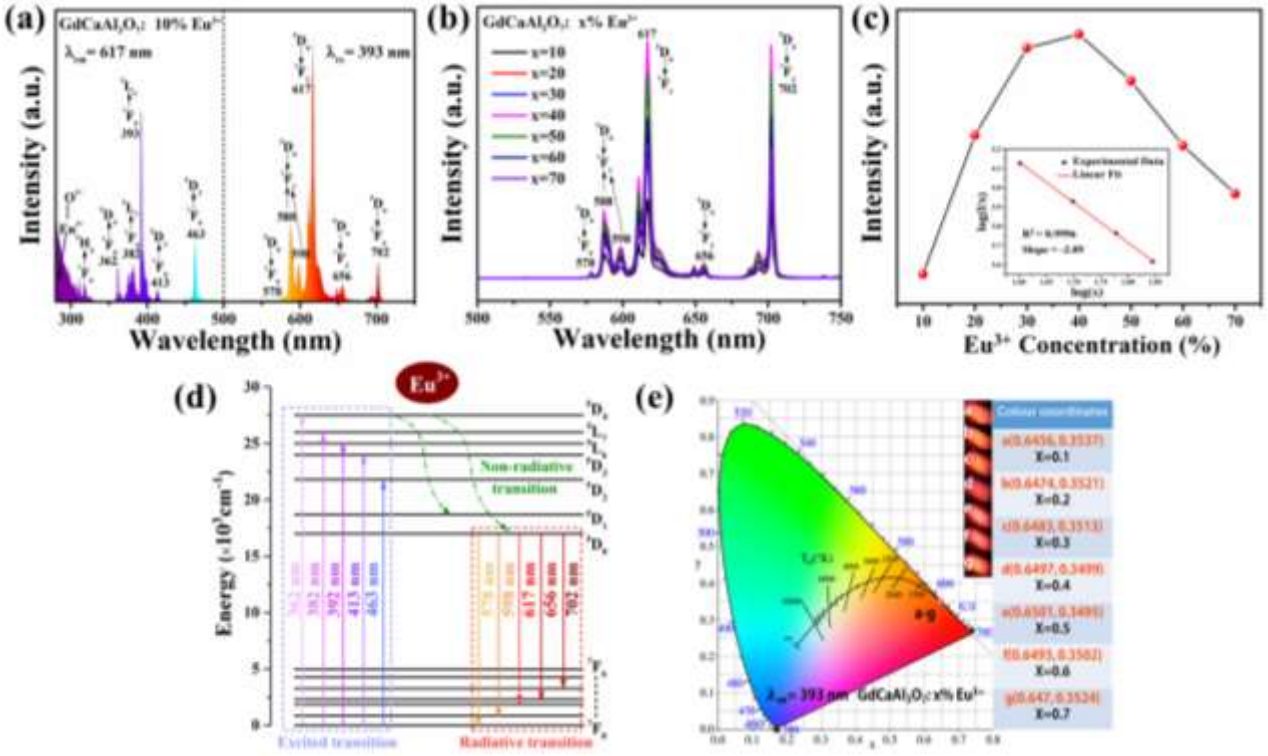


**Fig. 4** (a) Excitation and emission spectra of $GdCaAl_3O_7$: 10% $Eu^{3+}$. (b) Emission spectra of $GdCaAl_3O_7$: x% $Eu^{3+}$ for various $Eu^{3+}$ concentrations. (c) Integrated emission intensity as a function of $Eu^{3+}$ concentrations. Inset: the plot of log(x) versus log(I/x). (d) Schematic energy level diagram for the possible transitions of $Eu^{3+}$ in $GdCaAl_3O_7$. (e) CIE chromaticity diagram and digital photograph of the $GdCaAl_3O_7$: x% $Eu^{3+}$ under NUV light.

The temperature-dependent emission of the $GdCaAl_3O_7$: 40% $Eu^{3+}$ were measured in order to investigate the thermal stability of phosphors for practical applications. In **Fig. 5a**, it can be found that the intensity of all the peaks decreased with increasing the temperatures in the range of 183-423 K due to the well-known thermal quenching effects. **Fig. 5b** shows the normalized temperature-dependent emission intensity of the dominated transition ($^5D_0 \rightarrow {}^7F_2$). In general, the phosphor stability can be justified by comparing the emission intensity at 303 K with that at 423 K.[42] It can be seen that the emission intensity at 423 K retained 81.01% of that at 303 K, suggesting that the $GdCaAl_3O_7$: x% $Eu^{3+}$ have good thermal stability as a kind of red-emitting phosphors for solid-state lighting. In order to study the thermal quenching phenomenon, the activation energy ($\Delta E$)

was calculated by the following expression [43]:

$$I = \frac{I_0}{1+A*\exp(-\Delta E/kT)} \quad (4)$$

where $I_0$ and $I$ correspond to the emission intensity at the initial temperature (183 K) and $T$, respectively, $A$ is a constant related with the emission intensity, and $k$ is the Boltzmann constant ($8.6173 \times 10^{-5}\ eV/K$). In addition, the formula can be rewritten as below [26]:

$$In\left(\frac{I_0}{I}-1\right) = InA - \frac{\Delta E}{kT} \quad (5)$$

As displayed in **Fig. 5c**, it is obvious that all the experimental data were linear with a slope of $-0.163$, suggesting that the $\Delta E$ value for thermal quenching was about 0.163 eV in the $GdCaAl_3O_7$: 40% $Eu^{3+}$. Furthermore, the relationship between the activation energy and NR transition per unit time ($\alpha$) can be expressed as below [44]:

$$\alpha = s * \exp(\frac{-\Delta E}{kT}) \quad (6)$$

where $s$ is the frequency factor ($s^{-1}$). In this formula, it is reasonable to believe that the possibility of NR transition would be small and good thermal stability could be obtained when the activation energy was large. Herein, the activation energy (0.163 eV) of the $GdCaAl_3O_7$: 40% $Eu^{3+}$ was close to other single-doped $Eu^{3+}$ phosphors, such as $Ba_3Y_2B_6O_{15}$: $Eu^{3+}$ ($\Delta E = 0.16\ eV$) and $LiGdMgWO_6$: $Eu^{3+}$ ($\Delta E = 0.15\ eV$) [45,46].

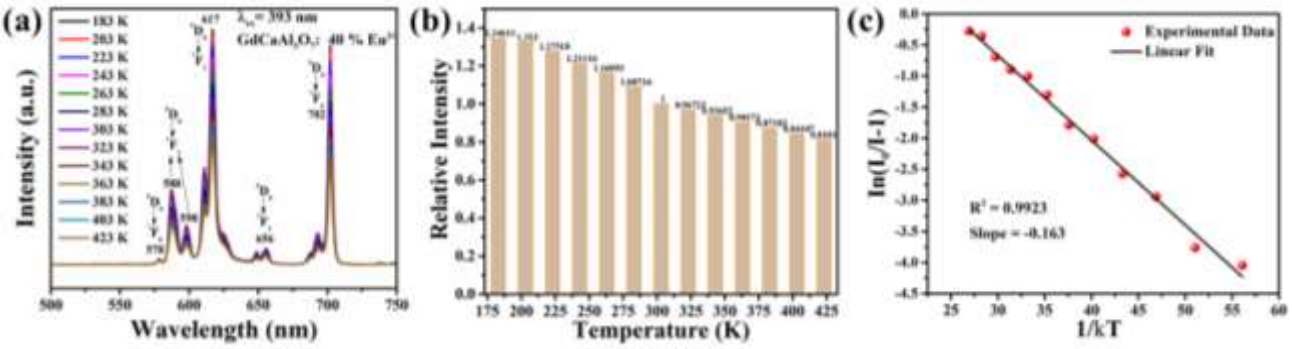


**Fig. 5** (a) Temperature-dependent emission spectra of $GdCaAl_3O_7$: 40% $Eu^{3+}$ and (b) normalized temperature-dependent integrated emission intensity of $^5D_0 \rightarrow {}^7F_2$ at various temperatures. (c) Plot of $\ln(I_0/I-1)$ versus 1/kT in the $GdCaAl_3O_7$: 40% $Eu^{3+}$.

### 3.3 Luminescent properties of $GdCaAl_3O_7$: y% $Tb^{3+}$

A series of $Tb^{3+}$ single-doped $GdCaAl_3O_7$ phosphors were fabricated and their emission spectra were tested. The excitation and emission spectra of the $GdCaAl_3O_7$: y% $Tb^{3+}$ are shown in **Fig. 6a**. Under 543 nm emission, it can be found that the excitation spectra had a broadband ranging from

230 nm to 296 nm with a maxima band at about 273 nm corresponding to the $4f^8$-$4f^75d^1$ transition of $Tb^{3+}$, and several sharp peaks at 304, 312, 340, 350 and 376 nm are assigned to the $^7F_6 \rightarrow {}^5H_6$, $^7F_6 \rightarrow {}^5H_7$, $^7F_6 \rightarrow {}^5L_6$, $^7F_6 \rightarrow {}^5L_9$ and $^7F_6 \rightarrow {}^5G_6$ transitions, respectively. It is noticeable that the strong absorption peak centered at 376 nm is due to the $^7F_6 \rightarrow {}^5G_6$ transition, indicating that the $GdCaAl_3O_7$: y% $Tb^{3+}$ can be well excited by the NUV lighting source. Under 376 nm excitation, the spectra exhibited the characteristic emissions of $Tb^{3+}$. The emission spectra included four major emission peaks centered at 492, 543, 587 and 620 nm as a result of the intra 4f-4f transition of $Tb^{3+}$. **Fig. 6b** shows the emission spectra for various $Tb^{3+}$-doped concentrations. The $^5D_4 \rightarrow {}^7F_5$ transition at around 543 nm was the dominate peak in the emission spectra, originating from magnetic dipole interaction. The highest emission intensity was found at 50% $Tb^{3+}$ doping concentration. When the doping concentration was more than this percent, the emission intensity decreased owing to the influence of concentration quenching, so the optimum doping concentration of $GdCaAl_3O_7$: y% $Tb^{3+}$ was believed as 50%. Meanwhile, in the emission spectra, no any overlaps were noticed, suggesting that the electric multipolar interaction dominated the concentration quenching. Furthermore, according to Eq. (3), the $Q$ value was calculated as 6.21 for the $GdCaAl_3O_7$: y% $Tb^{3+}$, which is close to 6, demonstrating that the dipole-dipole interaction dominated the concentration quenching in $GdCaAl_3O_7$: y% $Tb^{3+}$, as displayed in the inset of **Fig. 6c**.

In addition, the energy transfer among $Tb^{3+}$ in the $GdCaAl_3O_7$ host material was studied, as shown in **Fig. 6d**. Under 376 nm excitation, the $Tb^{3+}$ in the $^7F_6$ ground state can absorb pump photons and then transferred to the excited $^5H_6$, $^5H_7$, $^5L_6$, $^5L_9$ and $^5G_6$ level; secondly, the energy would be governed by dipole-dipole interaction and transferred from the excited level to the $^5D_4$ level by means of the non-radiative processes; Finally, The populated $^5D_4$ state would subsequently decay to the $^7F_6$, $^7F_5$, $^7F_4$ and $^7F_3$ states by radiative multiphoton relaxation steps, and generated four emissions centered at 492, 543, 587 and 620 nm following a relaxation to the ground state $^7F_6$, respectively. **Fig. 6e** shows the CIE chromaticity coordinate of $GdCaAl_3O_7$: y% $Tb^{3+}$ from (0.3893, 0.6011) to (0.3916, 0.5933). For the $GdCaAl_3O_7$: y% $Tb^{3+}$ phosphors, the phosphors emitted the brightest green light under NUV light source when the doping concentration of $Tb^{3+}$ was up to 50%, as presented in the inset of **Fig. 4e**. The result further demonstrates that the NUV light is a very appropriate excitation light source for the $GdCaAl_3O_7$: y% $Tb^{3+}$.

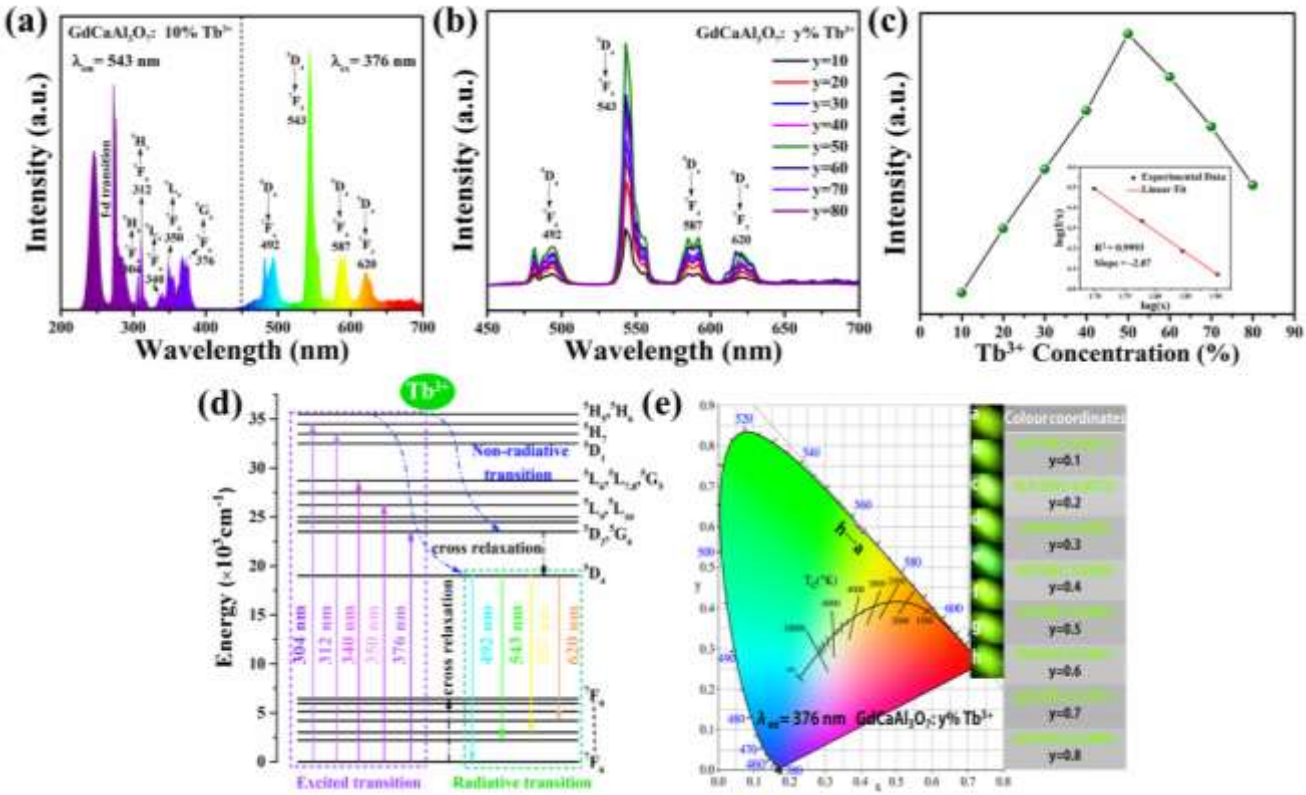


**Fig. 6** (a) Excitation and emission spectra of $GdCaAl_3O_7$: 10% $Tb^{3+}$. (b) Emission spectra of $GdCaAl_3O_7$: y% $Tb^{3+}$. (c) Emission intensity as a function of $Tb^{3+}$ concentrations. Inset: the plot of log(x) versus log(I/x). (d) Schematic energy level diagram for the possible transitions of $Tb^{3+}$ in $GdCaAl_3O_7$. (e) CIE chromaticity diagram and digital photograph of the $GdCaAl_3O_7$: y% $Tb^{3+}$ under NUV light.

The thermal stability of the $GdCaAl_3O_7$: 50% $Tb^{3+}$ was investigated based on the temperature-dependent emission spectra, as shown in **Fig. 7a**. Due to the thermal quenching effect, the emission intensity of the $GdCaAl_3O_7$: 50% $Tb^{3+}$ decreased with increasing the temperatures. The emission intensity still reached 81.36% at 423 K compared with that at 303 K, suggesting that the $GdCaAl_3O_7$: y% $Tb^{3+}$ have good thermal stability as green-emitting phosphors for solid-state lighting, as seen in **Fig. 7b**. In addition, in **Fig. 7c** the activation energy for this phosphor was calculated as 0.152 eV according to Eq. (5), which was slightly higher than other $Tb^{3+}$-doped phosphor materials, such as $Na_5Lu_9F_{32}$: $Tb^{3+}$ (0.14 eV) and $Sr_2Gd_8Si_6O_{26}$: $Tb^{3+}$ (0.13 eV) [47,48].

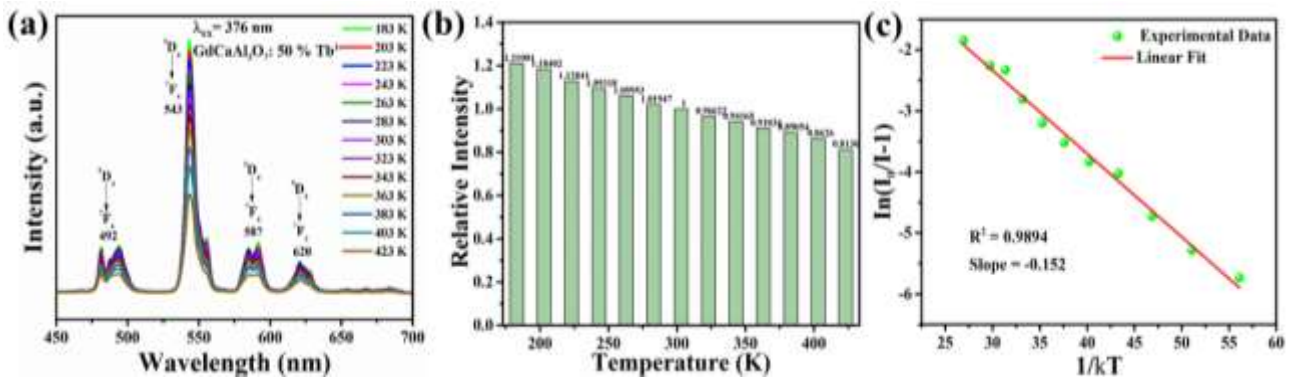


**Fig. 7** (a) Emission spectra and (b) normalized integrated emission intensity of $^5D_4 \rightarrow {}^7F_5$ for the $GdCaAl_3O_7$: 50% $Tb^{3+}$ as a function of temperature (183-453 K). (c) Plot of $\ln(I_0/I\text{-}1)$ versus 1/kT for the $GdCaAl_3O_7$: 50% $Tb^{3+}$ .

### 3.4 Luminescent properties of color-tunable $GdCaAl_3O_7$: x% $Eu^{3+}$@50% $Tb^{3+}$

As mentioned above, the optimum doping concentration of $Tb^{3+}$ in $GdCaAl_3O_7$ host lattices was 50%, which was selected to investigate the energy transfer in $Tb^{3+}$ and $Eu^{3+}$ co-doped $GdCaAl_3O_7$ host lattices. **Fig. 8a** showed the emission spectra of $GdCaAl_3O_7$: 50% $Tb^{3+}$@x% $Eu^{3+}$ (x= 1, 3, 5, 7, 9 and 11) under 376 nm excitation. The featured emission peaks of both $Tb^{3+}$ and $Eu^{3+}$ can be observed. Meanwhile, it can be seen that the intensity of the dominated peak ($^5D_4 \rightarrow {}^7F_5$) of $Tb^{3+}$ decreased with increasing the $Eu^{3+}$ concentrations, while the intensity of $Eu^{3+}$ emission peaks increased. On the other hand, the intensity of $Eu^{3+}$ reached the maximum when x was 3 and then nearly kept invariable due to the concentration quenching during the energy transfer, as shown in **Fig. 8b**. Consequently, the optimum doping concentration of $Eu^{3+}$ was 3% in $GdCaAl_3O_7$: 50% $Tb^{3+}$@x% $Eu^{3+}$. The ET efficiency ($\eta_T$) from $Tb^{3+}$ to $Eu^{3+}$ ions was estimated by the direct way as following expression [49]:

$$\eta_T = 1 - \frac{I_S}{I_{S0}} \tag{7}$$

Here, $I_S$ and $I_{S0}$ are the emission intensities of the single-doped $Tb^{3+}$ and co-doped $Tb^{3+}$@$Eu^{3+}$, respectively. Therefore, it can be calculated that the ET efficiency reached 93.65% when x was 11, as shown in **Fig. 8c**. The energy transfer diagram for the $GdCaAl_3O_7$: 50% $Tb^{3+}$@x% $Eu^{3+}$ in **Fig. 8d** illustrated the ET processes between $Tb^{3+}$ and $Eu^{3+}$ in $GdCaAl_3O_7$ host material. Under 376 nm irradiation, the energy would be transferred from the ground state of $^7F_6$ of $Tb^{3+}$ to the $^5G_6$ level, and then jumped to the $^5D_4$ level by non-radiative transition. In the meantime, the energy would be transferred from the higher $^5D_4$ ($Tb^{3+}$) level to the lower $^5D_0$ ($Eu^{3+}$) level, emitting the characteristic light of $Eu^{3+}$. Thus, it is reasonable to believe that the energy transfer from the $Tb^{3+}$ to $Eu^{3+}$ was

feasible and the ET efficiency was high. The CIE chromaticity coordinates of the $GdCaAl_3O_7$: 50% $Tb^{3+}$@x% $Eu^{3+}$ were calculated, as shown in **Fig. 8e**. It is noticeable from the digital images that the $GdCaAl_3O_7$: 50% $Tb^{3+}$@x% $Eu^{3+}$ could turn from greenish yellow, yellow, yellowish orange to near-red emission with increasing $Eu^{3+}$ contents under NUV light, indicating that the emission color of the phosphors could changed significantly. The result indicates that the as-obtained $GdCaAl_3O_7$: 50% $Tb^{3+}$@x% $Eu^{3+}$ phosphors are color-tunable, which have advantages of polychromatic light emissions under a single wavelength light and have promising applications as multicolor phosphors for white LEDs devices.

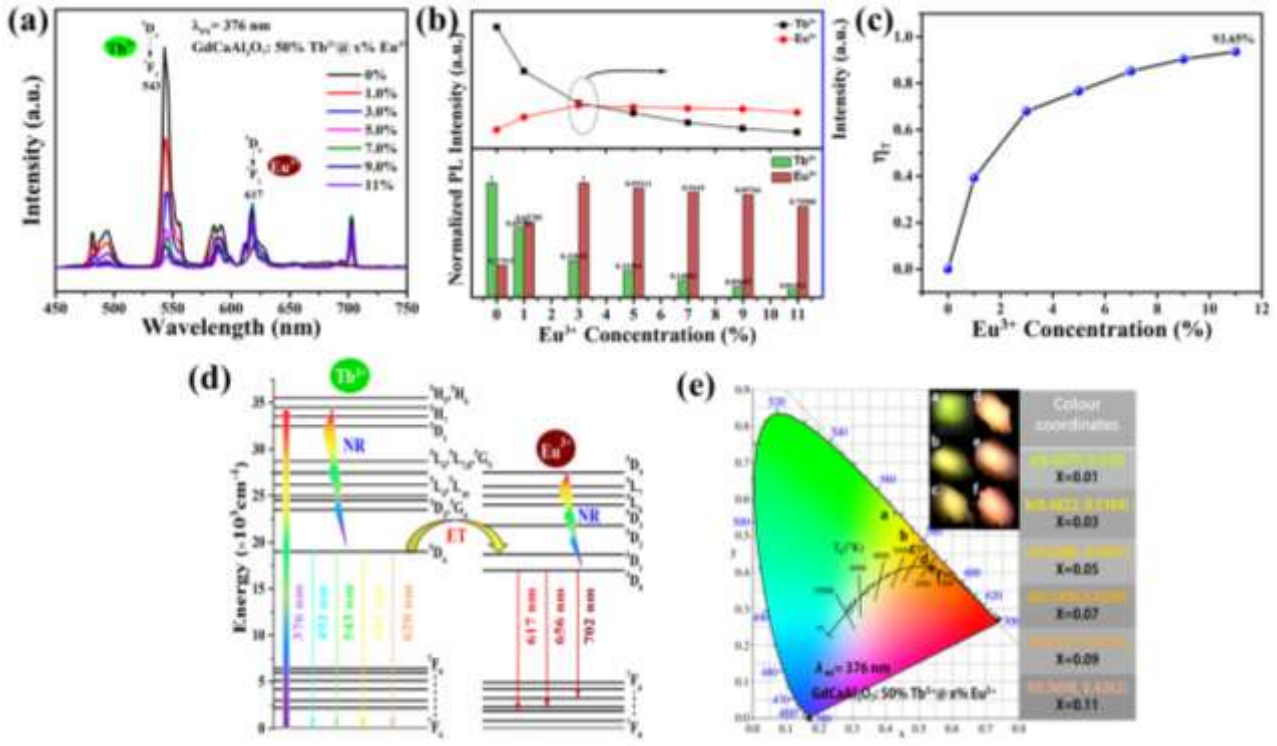


**Fig. 8** (a) PL emission spectra of the $GdCaAl_3O_7$: 50% $Tb^{3+}$@x% $Eu^{3+}$. (b) Normalized PL emission intensity of $^5D_4 \rightarrow {}^7F_5$ ($Tb^{3+}$) and $^5D_0 \rightarrow {}^7F_2$ ($Eu^{3+}$) transitions. (c) Energy transfer efficiency from $Tb^{3+}$ to $Eu^{3+}$ as a function of $Eu^{3+}$ concentrations. (d) Energy transfer from $Tb^{3+}$ to $Eu^{3+}$ in the $GdCaAl_3O_7$: 50% $Tb^{3+}$@x% $Eu^{3+}$. (e) CIE chromaticity coordinates of the $GdCaAl_3O_7$: 50% $Tb^{3+}$@x% $Eu^{3+}$. Inset: the digital photo images of phosphors under NUV light.

As mentioned above, the concentration quenching phenomenon was produced in $GdCaAl_3O_7$: 50% $Tb^{3+}$@x% $Eu^{3+}$ and was different from $Eu^{3+}$ single-doped $GdCaAl_3O_7$. The electric multipolar interaction was responsible for the concentration quenching during the ET processes. The relationship between exchange and multipolar interaction during the ET processes can be defined as follows [49]:

$$I_{S0}/I_S \propto C^{n/3} \quad (8)$$

In this formula, $I_{S0}$ and $I_S$ have the same meaning as Eq. (7), $C$ stands for the sum of $Tb^{3+}$ and $Eu^{3+}$, and $n$ has the same meaning as $Q$ of Eq. (3). The dependence of $I_{S0}/I_S$ on $C^{n/3}$ in $GdCaAl_3O_7$: 50% $Tb^{3+}$@x% $Eu^{3+}$ was investigated in **Fig. 9a-c**. It is obvious that the best linear relationship was $n = 10$, indicating that the ET processes was dominated by quadrupole-quadrupole interaction in $GdCaAl_3O_7$: 50% $Tb^{3+}$@x% $Eu^{3+}$.

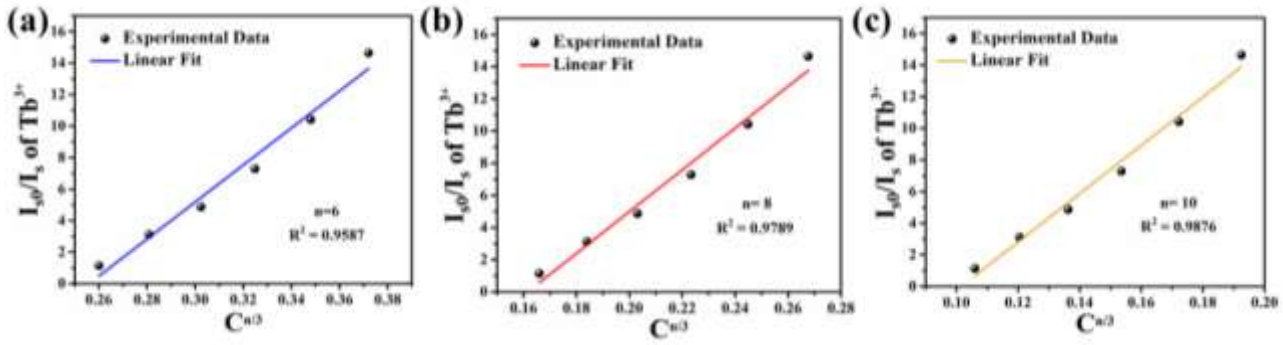


**Fig. 9** Dependence of $I_{S0}/I_S$ on $C^{n/3}$ in $GdCaAl_3O_7$: 50% $Tb^{3+}$@x% $Eu^{3+}$ when (a) $n = 6$, (b) $n = 8$ and (c) $n = 10$.

The thermal stability of PL emission intensity of the $GdCaAl_3O_7$: 50% $Tb^{3+}$@x% $Eu^{3+}$ was recorded under 376 nm excitation, as shown in **Fig. 10a**. The dominated and sharp peak of the $^5D_4 \rightarrow {}^7F_5$ ($Tb^{3+}$) transition confirmed the thermal stability of $Tb^{3+}$@$Eu^{3+}$ co-doped phosphors, while the PL emission intensity decreased with increasing the temperatures as similar with the single-doped samples. The emission intensity could reach 79.9% at 423 K in comparison to the initial intensity (183 K), as displayed in **Fig. 10b**, corresponding to 81.01% level of $Eu^{3+}$ single-doped sample and 81.36% level of $Tb^{3+}$ single-doped sample. The activation energy was calculated as 0.157 eV which is higher than the single-doped $GdCaAl_3O_7$: 50% $Tb^{3+}$ (0.152 eV), but lower than that of $GdCaAl_3O_7$: 40% $Eu^{3+}$ (0.163 eV), suggesting that the thermal stability of $Eu^{3+}$@$Tb^{3+}$ co-doped $GdCaAl_3O_7$ located in between $Eu^{3+}$ and $Tb^{3+}$ single-doped $GdCaAl_3O_7$.

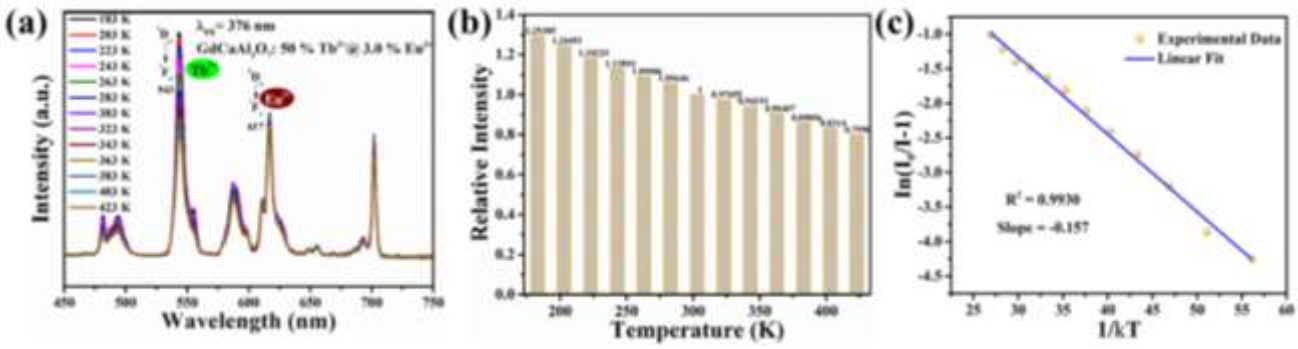


**Fig. 10** (a) Temperature-dependent PL emission spectra, (b) normalized PL emission intensity and (c) plot of ln ($I_0$/I-1) versus 1/kT in the $GdCaAl_3O_7$: 50% $Tb^{3+}$@3.0% $Eu^{3+}$.

### 3.5 Decay times of $GdCaAl_3O_7$: 50% $Tb^{3+}$@x% $Eu^{3+}$

The decay curves of the obtained $GdCaAl_3O_7$: 50% $Tb^{3+}$@x% $Eu^{3+}$ (x= 0, 1, 3, 5, 7 and 11) were recorded by monitoring 376 nm excitation and 543/617 nm emission, as shown in **Fig. 11a-b**. The relation between luminescent intensity and lifetime can be defined as below [38]:

$$I_{(t)} = I_0 + A_1 \exp\left(-\frac{t}{\tau_1}\right) \quad (9)$$

where $A_1$ is the constant and $\tau_1$ is related to the lifetime, $I_{(t)}$ and $I_0$ are the PL intensity at time t and initial time, respectively. It can be found that the experimental data can be well-fitted by a single exponential function. According to the Eq. (9), the corresponding lifetimes of $GdCaAl_3O_7$: 50% $Tb^{3+}$@x% $Eu^{3+}$ at the monitoring mode of 543 nm emission and 376 nm excitation were determined as approximately 6.43, 5.72, 2.28, 2.05, 1.46, 1.32 and 1.08 ms when x was 1, 3, 5, 7, 9 and 11, respectively. Meanwhile, the decay times at the monitoring mode of 617 nm emission and 376 nm excitation were 3.19, 4.23, 4.14, 3.63, 3.41, and 3.32 ms when x was 1, 3, 5, 7, 9 and 11, respectively. It further demonstrates that the optimal doping concentration of $Eu^{3+}$ is 3 mol%. From the obtained lifetime values, it is clear that the lifetime of $Tb^{3+}$ ($^5D_4 \rightarrow {}^7F_5$) decreased with increasing the $Eu^{3+}$ concentration owing to the existed channels during the ET mechanism (quadrupole-quadrupole interaction) from $Tb^{3+}$ to $Eu^{3+}$ in $GdCaAl_3O_7$ host lattice. In order to demonstrate the existed ET process between $Tb^{3+}$ and $Eu^{3+}$, the ET efficiency was also be estimated as below [50]:

$$\eta_T = 1 - \frac{\tau}{\tau_0} \quad (10)$$

where the $\tau$ and $\tau_0$ correspond to the decay lifetimes of the single-doped $Tb^{3+}$ and co-doped $Tb^{3+}$@$Eu^{3+}$, respectively. Hence, ET efficiency based on the indirect way was estimated as 83.20% when the $Eu^{3+}$ was 11%. On the other hand, the ET rate in ET processes can be calculated based on

the decay lifetime, which can be defined as [51]:

$$p = \frac{1}{\tau} - \frac{1}{\tau_0} \tag{11}$$

Therefore, the ET rates from $Tb^{3+}$ to $Eu^{3+}$ of the $GdCaAl_3O_7$: 50% $Tb^{3+}$@x% $Eu^{3+}$ (x= 0, 1, 3, 5, 7 and 11) were calculated to be 0, 1.93, 28.31, 33.23, 52.94, 60.26 and 77.04%, respectively. It is noted that the ET rate had an upward tendency with increasing $Eu^{3+}$ concentrations, further indicating that the ET efficiency from $Tb^{3+}$ to $Eu^{3+}$ in $GdCaAl_3O_7$ host lattice was valid.

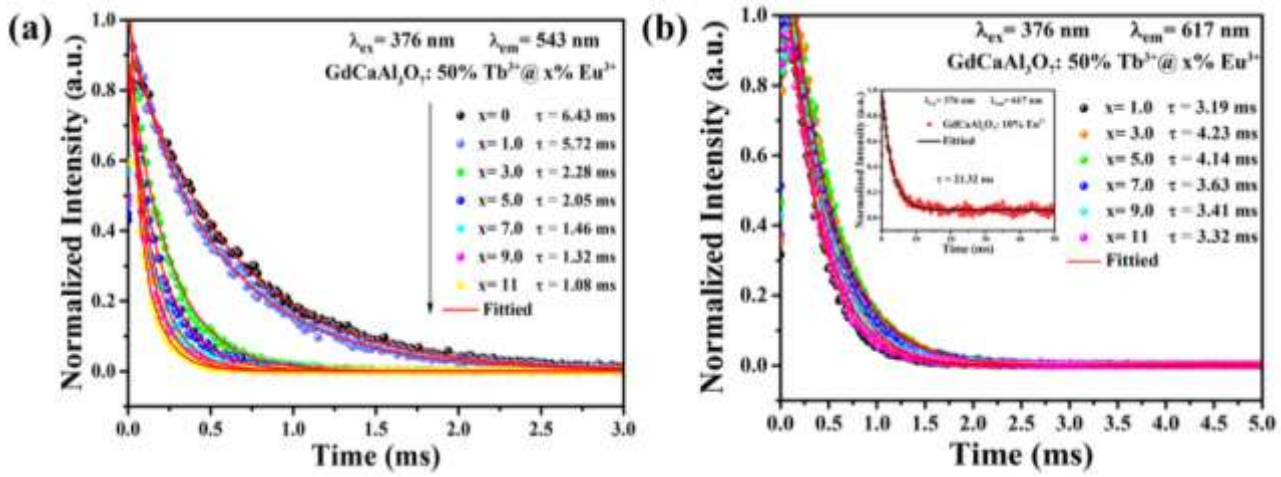


**Fig. 11** Decay curves of the $GdCaAl_3O_7$: 50% $Tb^{3+}$@x% $Eu^{3+}$ (x= 1, 3, 5, 7, 9 and 11) monitored at (a) 543 nm emission and (b) 617 nm emission under the excitation of 376 nm.

### 3.6 Electroluminescence (EL) properties of the designed white-LED lamp.

As discussed above, the CIE chromaticity coordinate of $GdCaAl_3O_7$: 50% $Tb^{3+}$@3.0% $Eu^{3+}$ sample was close to the warm white region. In this regard, by combining the NUV (~365 nm) chip with the $GdCaAl_3O_7$: 50% $Tb^{3+}$@3.0% $Eu^{3+}$ and BAM: $Eu^{2+}$ commercial phosphors, a white-LED device was fabricated, and the obtained color rendering index (CRI) and correlated color temperature (CCT) values were compared, as shown in **Fig. 12a** and **Fig. 12b**, respectively. It can be found that the EL spectra of fabricated $GdCaAl_3O_7$: 50% $Tb^{3+}$@3.0% $Eu^{3+}$ LED device emitted the characteristic peaks of $Tb^{3+}$ and $Eu^{3+}$ under a forward current of 100 mA, exhibiting a warm white glow. The CIE chromaticity coordinate was (0.3910, 0.3376), and the CCT and CRI value were 3348 K and 86.3, respectively, demonstrating that the color-tunable $GdCaAl_3O_7$: 50% $Tb^{3+}$@3% $Eu^{3+}$ phosphors are suitable for warm white-LED devices for indoor illumination.

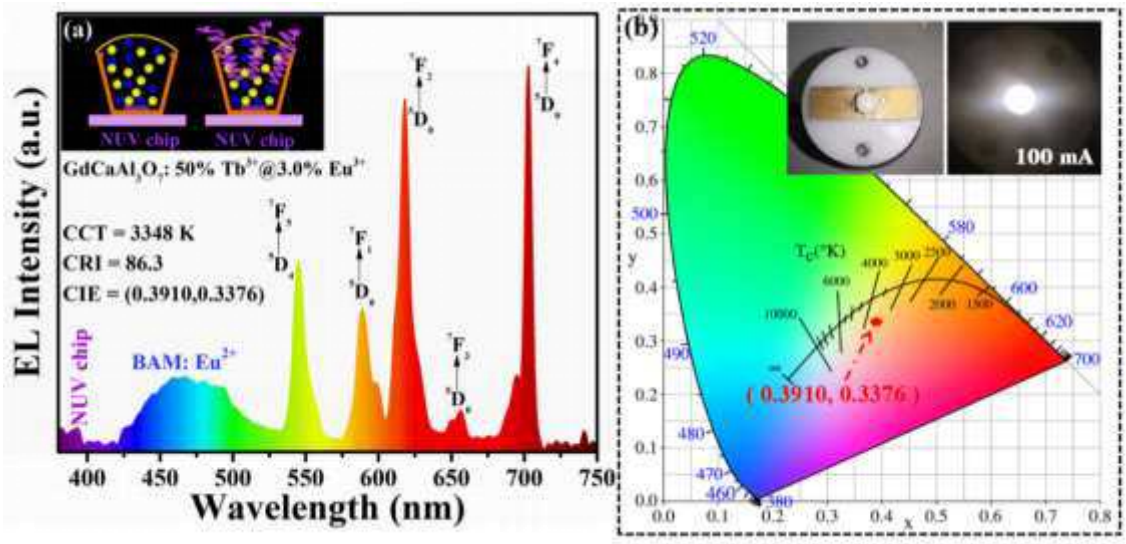


**Fig. 12** (a) EL emission spectra of the $GdCaAl_3O_7$: 50% $Tb^{3+}$@3.0% $Eu^{3+}$ by combining with BAM: $Eu^{2+}$ on a NUV (~365 nm) chip. Inset: a schematic diagram for the preparation of white LED device. (b) CIE chromaticity diagram of prepared white-LEDs. Inset: the photographs of the packaged LED devices with injection current of 100 mA.

## 4. Conclusions

In summary, the $GdCaAl_3O_7$: $RE^{3+}$ (RE=Eu, Tb, Eu@Tb) phosphors with particle sizes of 50-300 nm were successfully prepared by a sol-gel auto-combustion synthesis method. The SEM images indicated that the obtained products present honeycomb-like structure with many irregular continuous pores due to the releasing of a large amount of gas during the auto-combustion process. The EDS results suggest that $Eu^{3+}$ and $Tb^{3+}$ were well incorporated into the host matrices of $GdCaAl_3O_7$. All the $GdCaAl_3O_7$: $RE^{3+}$ (RE=Eu, Tb, Eu@Tb) products presented the characteristic emission of doped $RE^{3+}$. The optimum doping concentration of $Eu^{3+}$ was 3% in $GdCaAl_3O_7$: 50% $Tb^{3+}$@x% $Eu^{3+}$. The thermal stability of luminescence of $Eu^{3+}$@$Tb^{3+}$ co-doped $GdCaAl_3O_7$ located in between $Eu^{3+}$ or $Tb^{3+}$ single-doped $GdCaAl_3O_7$. The fabricated light-emitting diode (LED) device can emit glaring warm white light with high CRI (86.3) and low CCT (3348 K). These results indicated that the prepared co-doped $GdCaAl_3O_7$: $Eu^{3+}$@$Tb^{3+}$ phosphors were suitable for indoor illumination.

## Acknowledgements

This work is supported by Natural Science Foundation of China (No.51701098) and Natural Science Foundation of Ningbo Municipality (No. 2019A610064). This work is also sponsored by K. C. Wong Magna Foundation in Ningbo University.

## References


[1] Hua Y, Yu JS. Broadband near-ultraviolet excited $La_2Mo_2O_9:Eu^{3+}$ red-emitting phosphors with high color purity for solid-state lighting. *J Alloys Compd* 2019, **783**: 969-976.

[2] Xie M, Wei H, Wu W. Site occupancy studies and luminescence properties of emission tunable phosphors $Ca_9La(PO_4)_7$:Re (Re = $Ce^{3+}$, $Eu^{2+}$). *Inorg Chem* 2019, **58**: 1877-1885.

[3] Zhang W, Shen H, Hu XL, Wang Y, Li JF, Zhu ZJ, You ZY, Tu CY. Solid-state synthesis, structure and spectroscopic analysis of Dy:$CaYAl_3O_7$ phosphors. *J Alloys Compd* 2019, **781**: 255-260.

[4] Zhou L, Du P, Li W, Luo L. Lithium ion doping triggered splendid quantum efficiency and thermal stability in $Li_2SrSiO_4$:$xEu^{2+}$ phosphors for optical thermometry and high luminous efficiency white-LED. *New J Chem* 2019, **43**: 16445.

[5] Huang X, Guo H, Sun L, Thangavel S, Wu Y. A high-efficiency, broadband-excited cyan-emitting $Ba_3Lu_2B_6O_{15}:Ce^{3+},Tb^{3+}$ phosphor for near-UV-pumped white light emitting diodes. *J Alloys Compd* 2019, **787**: 865-871.

[6] Sayed AK, Abdul J, Qudrat UK, Rana MI, Ikhtisham M, Karim K, Maryam K, Dong B, Noor ZK, Yu JL, Zhu L, Simeon A. New physical insight into crystal structure, luminescence and optical properties of $YPO_4:Dy^{3+}$\$Eu^{3+}$\$Tb^{3+}$ single-phase white-light-emitting phosphors. *J Alloys Compd* 2020, **817**: 152687.

[7] Shi Y, Zhu G, Masayoshi M, Yasuo S, Wang Y. Color-tunable $LaCaAl_3O_7:Ce^{3+}$, $Tb^{3+}$ phosphors for UV light-emitting diodes. *Mater Res Bull* 2013, **48**: 114–117.

[8] Sanjith U, Kyoung HL, Woon JC, Won BI. Full-color-emitting $CaYAl_3O_7$: $Pr^{3+}$, $Ce^{3+}$ phosphor for near-UV LED-based white light. *J Lumin* 2014**, 152**: 176–81.

[9] Shen B, Wu F, Zhang Y, Xia H, Chen B, Hu J. Multicolour emission from thermally stable $Tb^{3+}/Eu^{3+}$ co-doped $CaLa_4Si_3O_{13}$ phosphors for single-component w-LEDs application. *J Alloys Compd* 2019, **809**, 151836.

[10] Hong F, Cheng H, Song C, Liu G, Yu W, Wang J, Dong X. Novel polygonal structure $Mn^{4+}$ activated $In^{3+}$-based Elpasolite-type hexafluorides red phosphor for warm white light-emitting diodes (WLEDs). *Dalton T* 2019, **78**: 1376-1385.

[11] Luo X, Ji YA, Soo HK. Aerosol synthesis and luminescent properties of $CaAl_2O_4:Eu^{2+}$, $Nd^{3+}$ down-conversion phosphor particles for enhanced light harvesting of dye-sensitized solar cells. *Sol Energy* 2019, **178**: 173-180.

[12] Sonika K, Sitender S, Suman S, Anura S, Bernabe M, Devender S. Synthesis and Optoelectronic Characteristics of $MGdAl_3O_7:Eu^{3+}$ Nanophosphors for Current Display Devices. *T Indian Ceram Soc* 2019, **78**: 219-226.

[13] Zhou L, Wallace CH, Choy, Shi J, Gong M, Liang H. Synthesis and luminescent properties of $GdSrAl_3O_7:Tb^{3+}$ phosphor under VUV/UV excitation. *J Alloys Compd* 2008, **463**: 302–305.

[14] Liu Q, Li X, Guo J, Wang L, Song J, Zhang Q. Second-order John-Teller distortion in the thermally stable Li (La, Gd)$MgWO_6:Eu^{3+}$ phosphor with high quantum efficiency. *Dyes Pigments* 2019, **160**: 165–171.

[15] Liao J, Liu S, Liu B, Nie L, Fu J, Wen H.-r. Sol–gel preparation and photoluminescence properties of $CaREAl_3O_7:Eu^{3+}$ (RE = Y, Gd, Lu) phosphors. *Optik* 2015, **126**: 3781–3785.

[16] Matos MG, Pereira PFS, Calefifi PS, Ciuffifi KJ, Nassar EJ. Preparation of a $GdCaAl_3O_7$ matrix by the non-hydrolytic sol–gel route. *J Lumin* 2009, **129**: 1120–1124.

[17] Bao A, Tao C, Yang H. Synthesis and luminescent properties of nanoparticles $GdCaAl_3O_7:RE^{3+}$ (RE = Eu, Tb) via the sol–gel method. *J Lumin* 2007, **126**: 859–865.

[18] Zhou L, Choy WCH, Shia J, Gong M, Liang H, Yuk TI. Synthesis, vacuum ultraviolet and near ultraviolet-excited luminescent properties of $GdCaAl_3O_7$: $RE^{3+}$ (RE = Eu, Tb). *J Solid State Chem* 2005, **178**: 3004–3009.

[19] Satyender PK, Sonika S, Sheetal L, Avni K, Vinod T. Photoluminescent Properties of $Tb^{3+}$ Doped $GdSrAl_3O_7$ Nanophosphor Using Solution Combustions Synthesis. *Electron Mater Lett* 2015, **11**: 409–415.

[20] Kale MA, Joshia CP, Moharil SV, Muthal PL, Dhopte SM. Luminescence in $LaCaAl_3O_7$ prepared by combustion synthesis. *J Lumin* 2008, **128**: 1225–1228.

[21] Singh S, Khatkar SP, Boora P, Taxak VB. Structural and luminescent properties of $Eu^{3+}$-doped $GdSrAl_3O_7$ nanophosphor. *J Mater Sci* 2014, **49**: 4773–4779.

[22] Du P, Ran W, Hou Y, Luo L, Li W. $Eu^{3+}$-Activated $NaGdF_4$ Nanorods for Near-Ultraviolet Light- Triggered Indoor Illumination. *ACS Appl Nano Mater* 2019, **2**: 4275−4285.

[23] Li J, Zhang Z, Li X, Xu Y, Ai Y, Yan J, Shi J, Wu M. Luminescence properties and energy transfer of $YGa_{1.5}Al_{1.5}(BO_3)_4$: $Tb^{3+}$, $Eu^{3+}$ as a multi-colour emitting phosphor for WLEDs. *J Mater Chem C* 2017, 5: 6294.

[24] Song M, Zhao W, Ran W, Xue J, Liu Y, Jung HJ. Multicolor tunable luminescence and energy transfer mechanism in a novel single-phase $KBaGd(WO_4)_3$:$Tb^{3+}$, $Eu^{3+}$ phosphor for NUV WLEDs. *J Alloys Compd* 2019, 803: 1063-1074.

[25] Anilkumar K, Damodaraiah S, Babu S, Prasad VR, Ratnakaram YC. Emission spectra and energy transfer studies in $Dy^{3+}$ and $Dy^{3+}$/$Eu^{3+}$ co-doped potassium fluorophosphate glasses for white light applications. *J Lumin* 2019, 205: 190–196.

[26] Lu Z, Meng Y, Wen L, Huang M, Zhou L, Liao L, He D. Double perovskite $Ba_2LaNbO_6$:$Mn^{4+}$, $Yb^{3+}$ phosphors: potential application to plant-cultivation LEDs. *Dyes Pigments* 2019, **160**: 395-402.

[27] Bao A, Tao C, Yang H. Luminescent properties of nanoparticles $LaSrAl_3O_7$:$RE^{3+}$ (RE = Eu, Tb) via the citrate sol–gel method. *J Mater Sci.-Mater El* 2008, **19**: 476–481.

[28] Bao A, Yang H, Tao C. Synthesis and luminescent properties of nanoparticles $LaSrAl_3O_7$:Eu, Tb. *Currr Appl Phys* 2009, **9**: 1252–1256.

[29] Bedyal AK, Ramteke DD, Kumar V, Swart HC. Excitation wavelength and $Eu^{3+}$/$Tb^{3+}$ content ratio dependent tunable photoluminescence from $NaSrBO_3$:$Eu^{3+}$/$Tb^{3+}$ phosphor. *J Mater Sci.-Mater El* 2019, **30**: 11714–11726.

[30] Wen D, Feng J, Li J, Shi J, Wu M, Su Q. $K_2Ln(PO_4)(WO_4)$:$Tb^{3+}$, $Eu^{3+}$ (Ln = Y, Gd and Lu) phosphors: highly efficient pure red and tuneable emission for white light-emitting diodes. *J Mater Chem C* 2015, **3**: 2107.

[31] Umer F, Sun X, Zhao Z, Raheel AJ, Gao C, Dai R, Wang Z, Zhang Z. Thermally stable $Na_{3.6}Y_{1.8}(PO_4)_3$: $Eu^{3+}$ phosphor, luminescent properties and application in WLEDs. *J Alloys Compd* 2020, **821**: 153513.

[32] Sheetal, Taxak VB, Mandeep, Khatkar SP. Synthesis, characterization and luminescent properties of Eu/Tb-doped $LaSrAl_3O_7$ nanophosphors. *J Alloys Compd* 2013, **549**: 135–140.

[33] Du P, Yu JS. $Eu^{3+}$-activated $La_2MoO_6$-$La_2WO_6$ red-emitting phosphors with ultrabroad excitation band for white light-emitting diodes. *Sci Rep* 2017, **7**: 11953.

[34] Vijay S, Hakeem DA, Lakshminarayana G, Singh PK, Kokate S. Investigation on luminescence properties of $CaLaAl_3O_7$ doped with $Sm^{3+}$ ions phosphors prepared by sol-gel procedure. *Optik* 2020, **206**: 164251.

[35] Ekambaram S, Patil KC, Maaza M. Synthesis of lamp phosphors: facile combustion approach. *J Alloys Compd* 2005, **393**: 81–92.

[36] Shi L, Han YJ, Zhang ZG, Ji ZX, Shi DC, Geng XY, Zhang H, Li M, Zhang ZW. Synthesis and photoluminescence properties of novel $Ca_2LaSbO_6$:$Mn^{4+}$ double perovskite phosphor for plant growth LEDs. *Ceram Int* 2019, **45**: 4739–4746.

[37] Hua Y, Hussain SK, Yu JS. Ultrafast preparation of Europium(III) and Terbium(III) activated $LaSr_2F_7$ nanoparticles for white LEDs and anti-counterfeiting mark. *J Alloys Compd* 2020, **826**: 154078.

[38] Chen X, Jiang L, Zhou L, He M, Li J, Wu A, Chen H. Up-conversion luminescence properties and energy

transfer mechanism of $SrAl_2B_2O_7$: $Er^{3+}$@$Yb^{3+}$ phosphors. *J Alloys Compd* 2020, **840**: 155489.

[39] Li K, Lian H, Van Deuna R, Brik MG. A far-red-emitting $NaMgLaTeO_6$:$Mn^{4+}$ phosphor with perovskite structure for indoor plant growth. *Dyes Pigments* 2019, **162**: 214–221.

[40] Li X, Yang C, Liu Q, Wang X, Mi X. Enhancement of luminescence properties of $SrAl_2Si_2O_8$: $Eu^{3+}$ red phosphor. *Ceram Int* 2020, **46**: 17376–17382.

[41] Zhang X, Shen T, Kan D, Zhang D, Dong R, An Z, Song Y, Zheng K, Sheng Y, Shi Z, Zou H. Study on the Local Structure and Luminescence Properties of a $Y_2Mg_2Al_2Si_2O_{12}$:$Eu^{3+}$ Red Phosphor for White-Light-Emitting Diodes. *Inorg Chem* 2020, **59**: 9927−9937.

[42] Xia M, Wu X, Zhong Y, Hintzen HT (Bert), Zhou Z, Wang J. Photoluminescence properties and energy transfer in a novel $Sr_8ZnY(PO_4)_7$:$Tb^{3+}$,$Eu^{3+}$ phosphor with high thermal stability and its great potential for application in warm white light emitting diodes. *J Mater Chem C* 2019, **7**: 2927-2935.

[43] Yang Z, Jia C, Zhang G, Han G, Wang H, Bu H, Tan X, Xu D, Sun J. Tunable blue-green color emission and energy transfer of $Sr_3NaSc(PO_4)_3F$:$Eu^{2+}$,$Tb^{3+}$ phosphors with near-UV broad band excited for white LEDs. *J Lumin* 2019, **206**: 585-592.

[44] Han JY, Im WB, Lee G, Jeon DY. Near UV-pumped yellow-emitting $Eu^{2+}$-doped $Na_3K(Si_{1-x}Al_x)_8O_{16\pm\delta}$ phosphor for white-emitting LEDs. *J Mater Chem C* 2012, **22**: 8793-8798.

[45] Annadurai G, Li B, Devakumar B, Guo H, Sun L, Huang X. Synthesis, structural and photoluminescence properties of novel orange-red emitting $Ba_3Y_2B_6O_{15}$:$Eu^{3+}$ phosphors. *J Lumin* 2019, **208**: 75–81.

[46] Liu Q, Li X, Guo J, Wang L, Song J, Zhang Q. Second-order John-Teller distortion in the thermally stable Li(La, Gd)$MgWO_6$:$Eu^{3+}$ phosphor with high quantum efficiency. *Dyes Pigments* 2019, **160**: 165-171.

[47] Yang J, Wu H, Song L, Wang X, Dong J, Gan S, Zou L. A novel synthesis route to monodisperse $Na_5Lu_9F_{32}$:$Tb^{3+}$ phosphors with superior thermal stability. *J Lumin* 2018, **204**: 533–538.

[48] Hussai SK, Rao GM, Raju GSR, Bharat LK, Rao PSVS, Yu JS. Photoluminescence and cathodoluminescence properties of $Sr_2Gd_8Si_6O_{26}$:$RE^{3+}$ ($RE^{3+}$=$Tb^{3+}$ or $Sm^{3+}$) phosphors. *J Lumin* 2016, **178**: 183–191.

[49] Zhou J, Xia Z. Luminescence color tuning of $Ce^{3+}$, $Tb^{3+}$ and $Eu^{3+}$ co-doped and tri-doped $BaY_2Si_3O_{10}$ phosphors via energy transfer. *J Mater Chem C* 2015, **3**: 7552-7560.

[50] Chen J, Song Y, Li D, Ma Q, Dong X, Yu W, Wang X, Yang Y, Wang J, Liu G. Investigating efficient energy transfer in novel strategy-obtained $Gd_2O_2S$:$Dy^{3+}$, $Eu^{3+}$ nanofibers endowed with white emitting and magnetic dual-functionality. *J Lumin* 2019, **206**: 509-517.

[51] Li L, Tang X, Wu Z, Zheng Y, Jiang S, Tang X, Xiang G, Zhou X. Simultaneously tuning emission color and realizing optical thermometry via efficient $Tb^{3+}$/$Eu^{3+}$ energy transfer in whitlockite-type phosphate multifunctional phosphors. *J Alloys Compd* 2019, **780**: 266-275.

# Figures

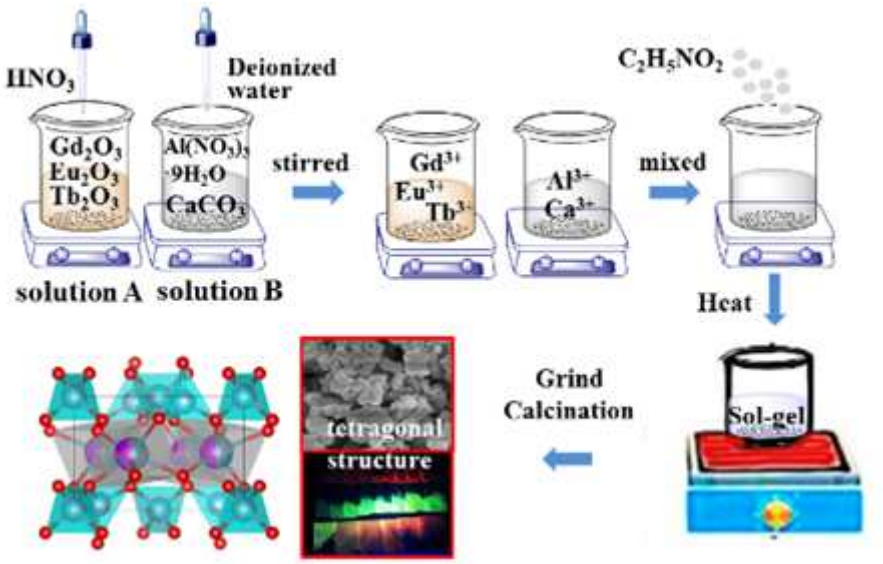


Figure 1

Schematic illustration of synthesis of GdCaAl3O7 phosphors doped with Eu3+ and Tb3+.

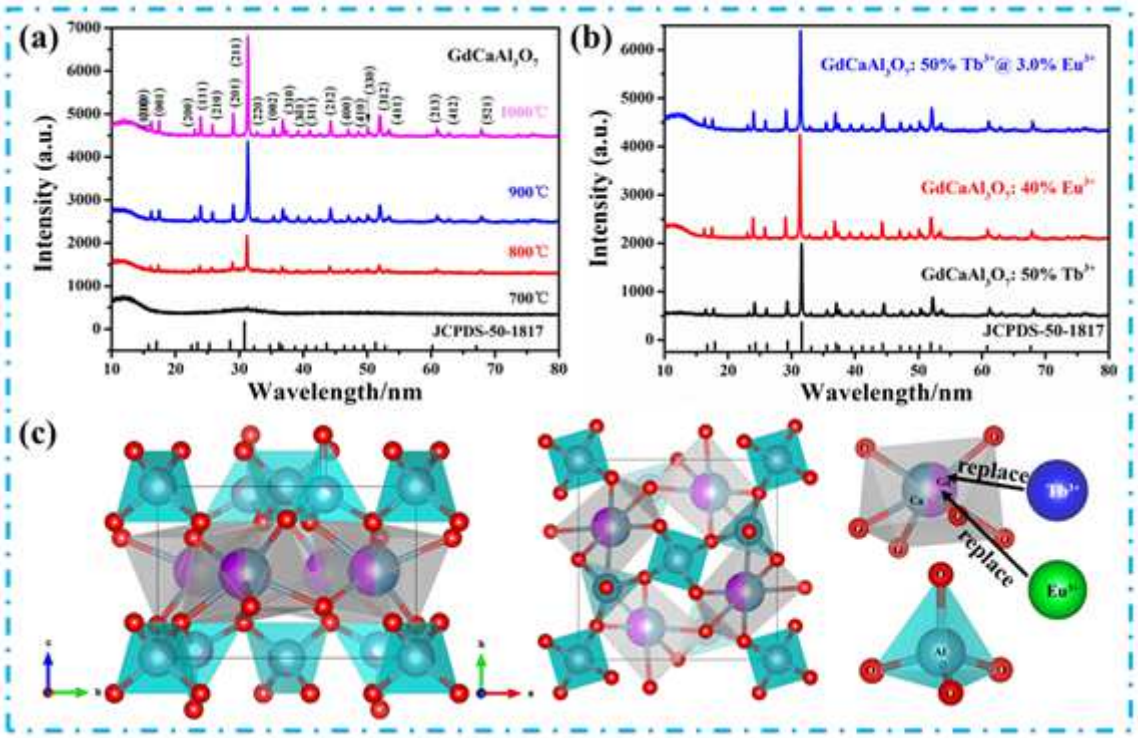


Figure 2

(a) XRD patterns of pure GdCaAl3O7 annealed at various temperatures. (b) XRD patterns of GdCaAl3O7: 50% Tb3+, GdCaAl3O7: 40% Eu3+ and GdCaAl3O7: 50% Tb3+@3.0% Eu3+ samples annealed at 1000 °C. (c) Crystal structure of GdCaAl3O7 unit cell (wherein Ca2+ and Gd3+ are located in octahedral; Al3+ are

located in tetrahedral; O2- are as coordinated ions; Eu3+ and Tb3+ ions substituted for Gd3+ on octahedral sites).

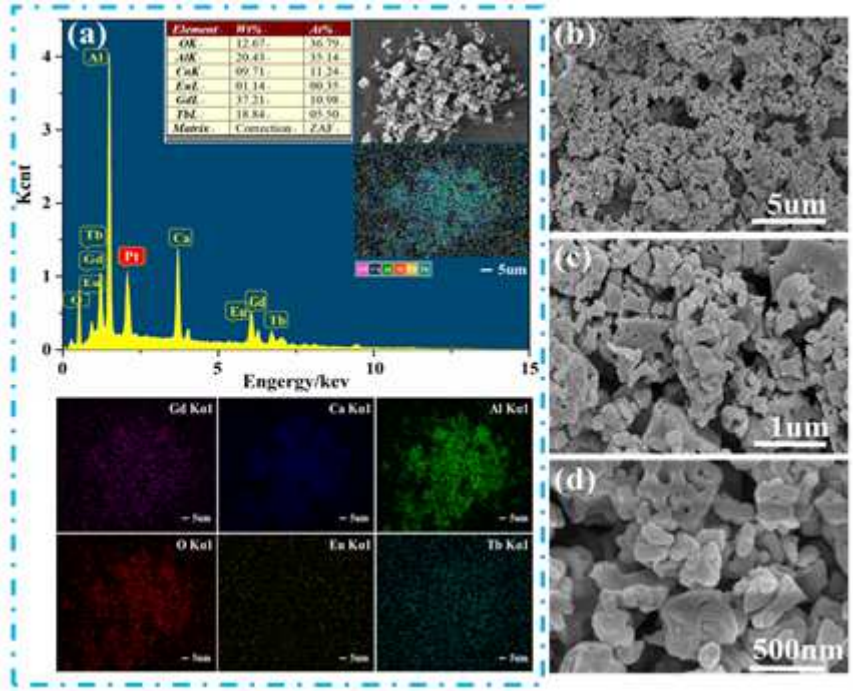


**Figure 3**

(a) EDS spectral patterns and elemental mapping images, (b-d) SEM images of GdCaAl3O7: 50% Tb3+@3.0% Eu3+ samples annealed at 1000 °C.

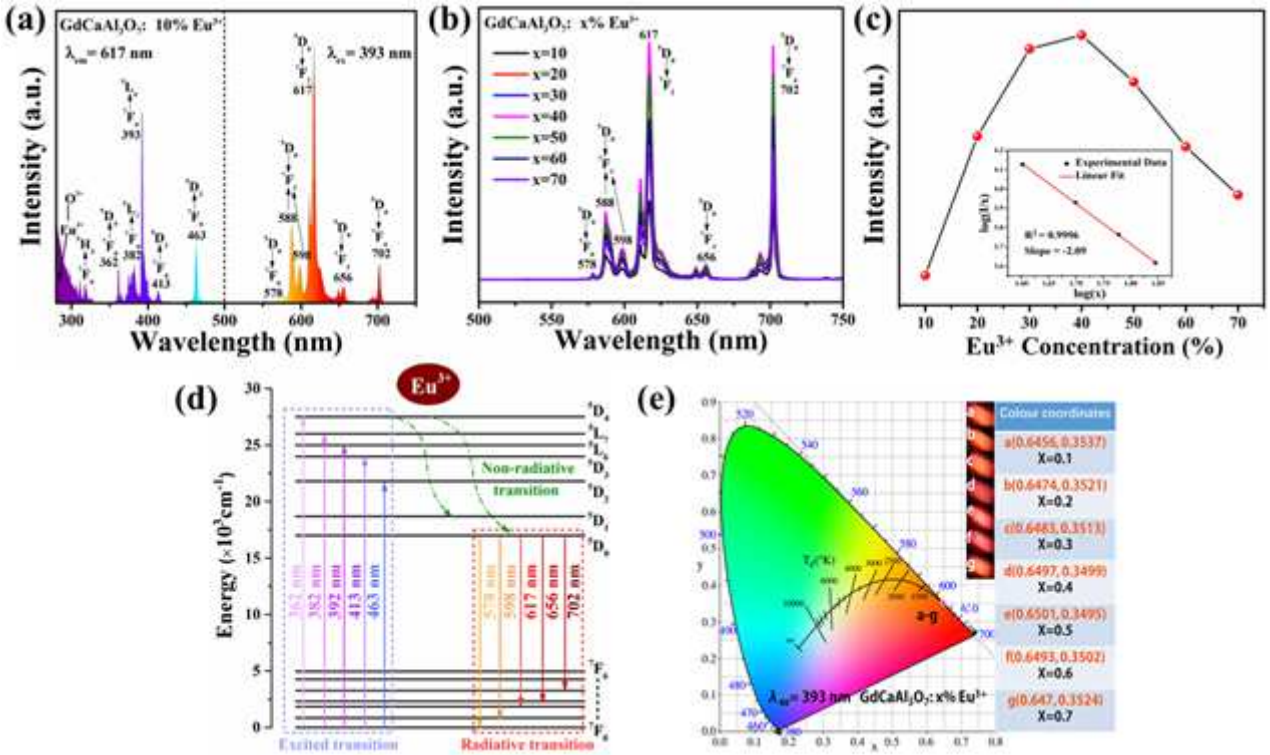


**Figure 4**

(a) Excitation and emission spectra of GdCaAl3O7: 10% Eu3+. (b) Emission spectra of GdCaAl3O7: x% Eu3+ for various Eu3+ concentrations. (c) Integrated emission intensity as a function of Eu3+ concentrations. Inset: the plot of log(x) versus log(I/x). (d) Schematic energy level diagram for the possible transitions of Eu3+ in GdCaAl3O7. (e) CIE chromaticity diagram and digital photograph of the GdCaAl3O7: x% Eu3+ under NUV light.

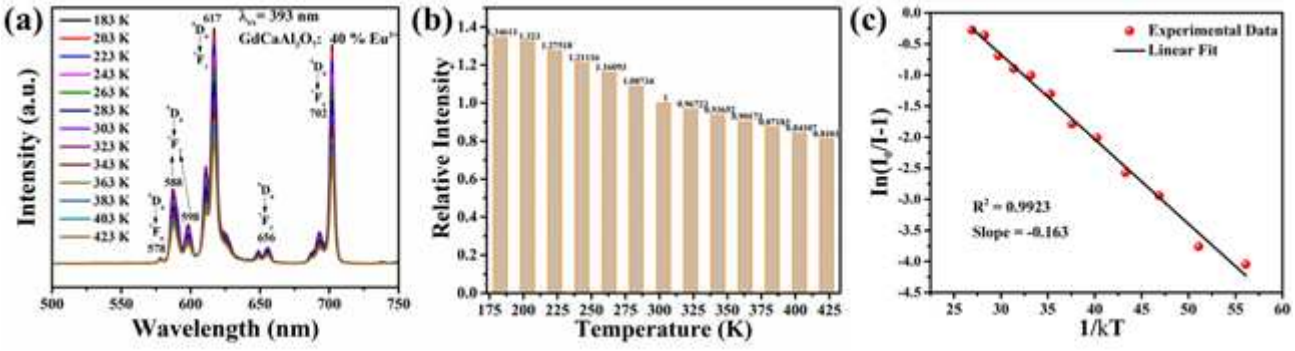


## Figure 5

(a) Temperature-dependent emission spectra of GdCaAl3O7: 40% Eu3+ and (b) normalized temperature-dependent integrated emission intensity of 5D0→7F2 at various temperatures. (c) Plot of ln(I0/I-1) versus 1/kT in the GdCaAl3O7: 40% Eu3+.

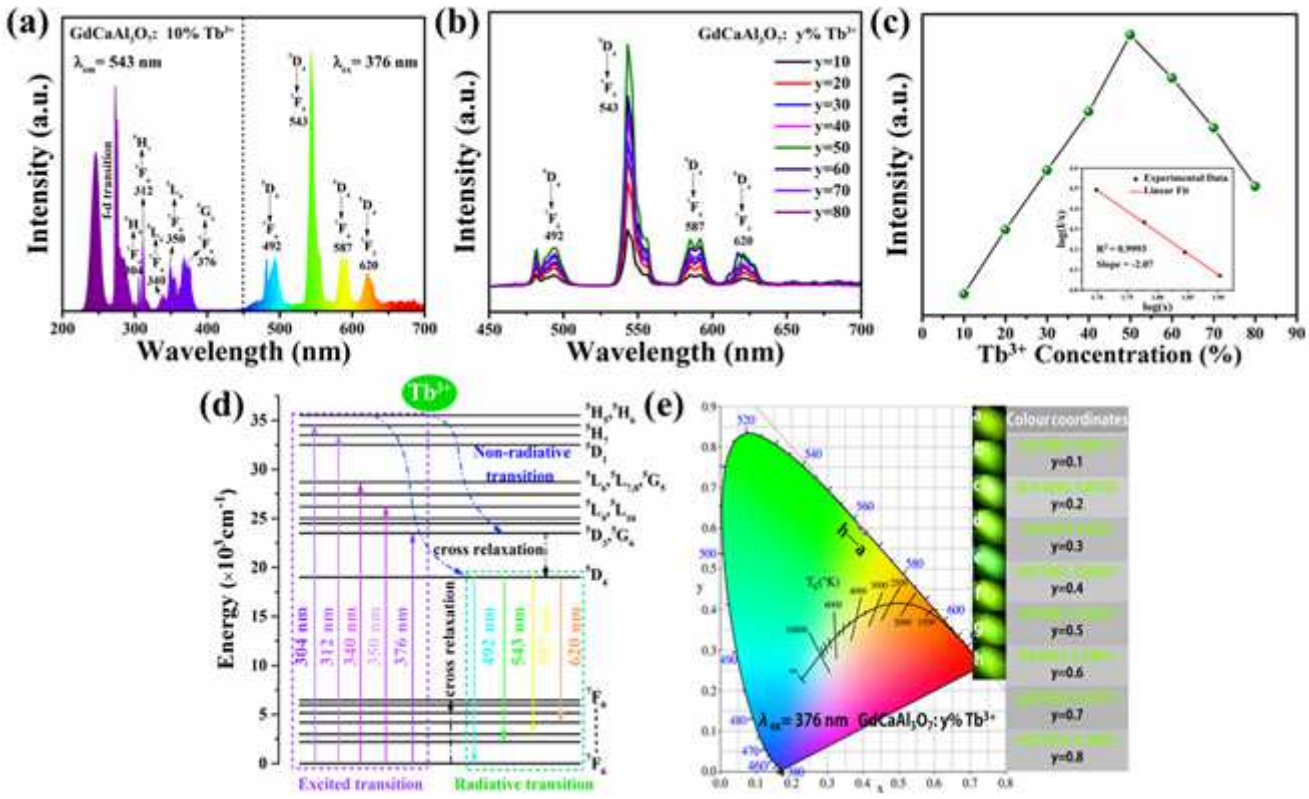


## Figure 6

(a) Excitation and emission spectra of GdCaAl3O7: 10% Tb3+. (b) Emission spectra of GdCaAl3O7: y% Tb3+. (c) Emission intensity as a function of Tb3+ concentrations. Inset: the plot of log(x) versus log(I/x).

(d) Schematic energy level diagram for the possible transitions of Tb3+ in GdCaAl3O7. (e) CIE chromaticity diagram and digital photograph of the GdCaAl3O7: y% Tb3+ under NUV light.

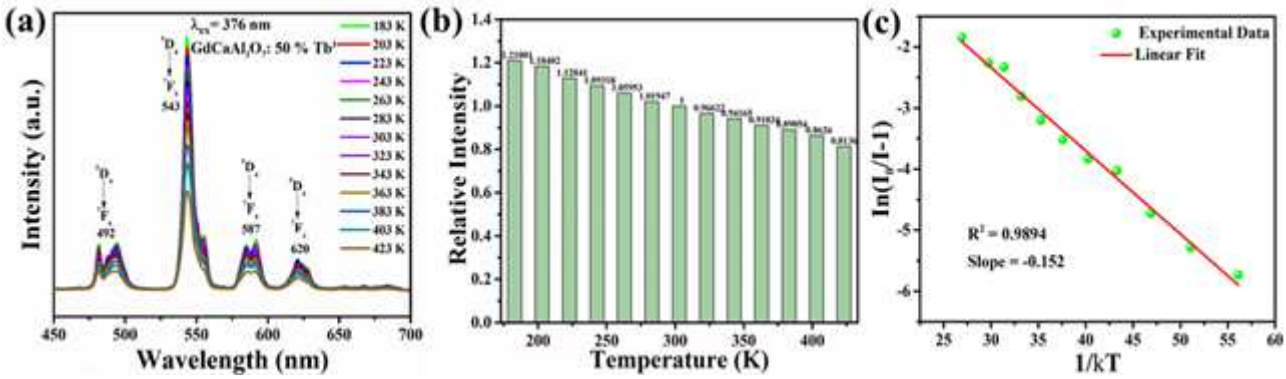


## Figure 7

(a) Emission spectra and (b) normalized integrated emission intensity of 5D4→7F5 for the GdCaAl3O7: 50% Tb3+ as a function of temperature (183-453 K). (c) Plot of ln(I0/I-1) versus 1/kT for the GdCaAl3O7: 50% Tb3+ .

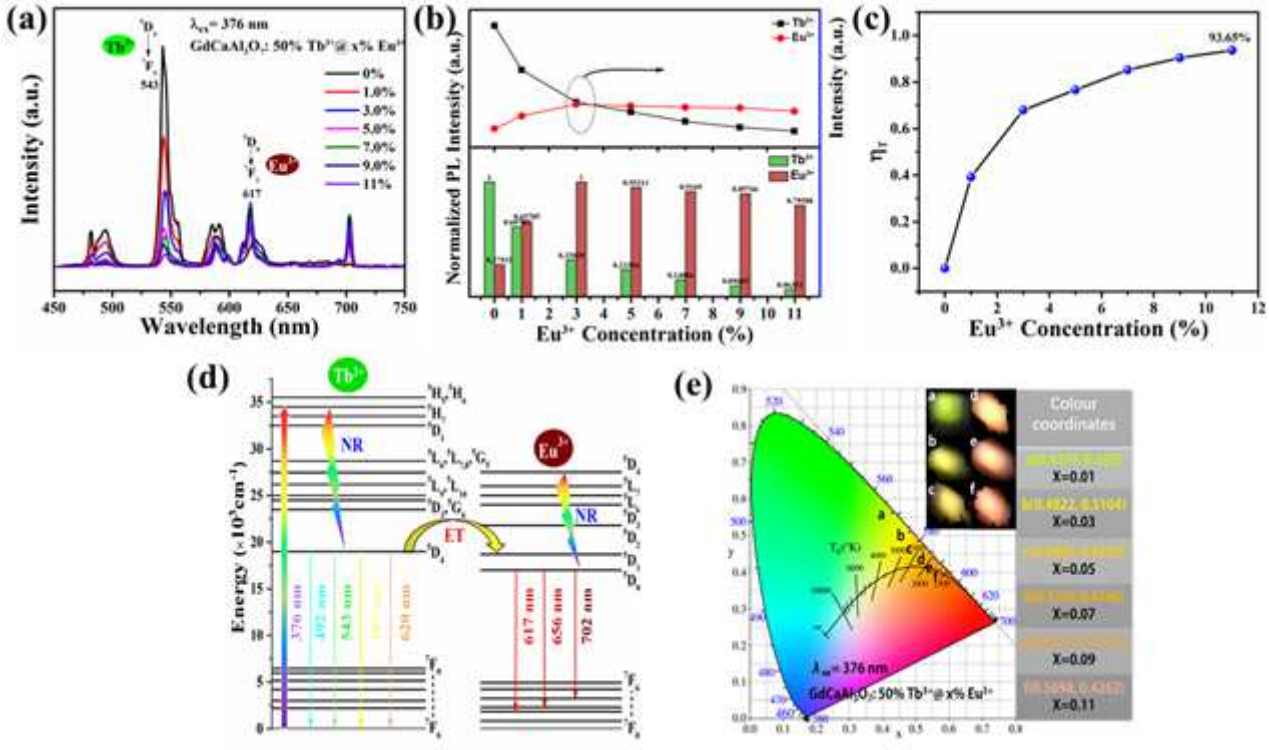


## Figure 8

(a) PL emission spectra of the GdCaAl3O7: 50% Tb3+@x% Eu3+. (b) Normalized PL emission intensity of 5D4→7F5 (Tb3+) and 5D0→7F2 (Eu3+) transitions. (c) Energy transfer efficiency from Tb3+ to Eu3+ as a function of Eu3+ concentrations. (d) Energy transfer from Tb3+ to Eu3+ in the GdCaAl3O7: 50% Tb3+@x% Eu3+. (e) CIE chromaticity coordinates of the GdCaAl3O7: 50% Tb3+@x% Eu3+. Inset: the digital photo images of phosphors under NUV light.

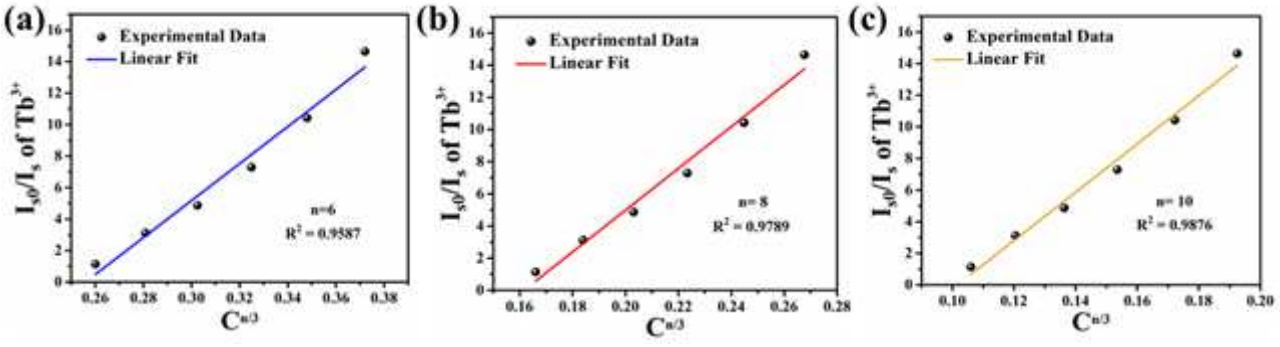


## Figure 9

Dependence of I_S0/I_S on Cn/3 in GdCaAl3O7: 50% Tb3+@x% Eu3+ when (a) n=6, (b) n=8 and (c) n=10.

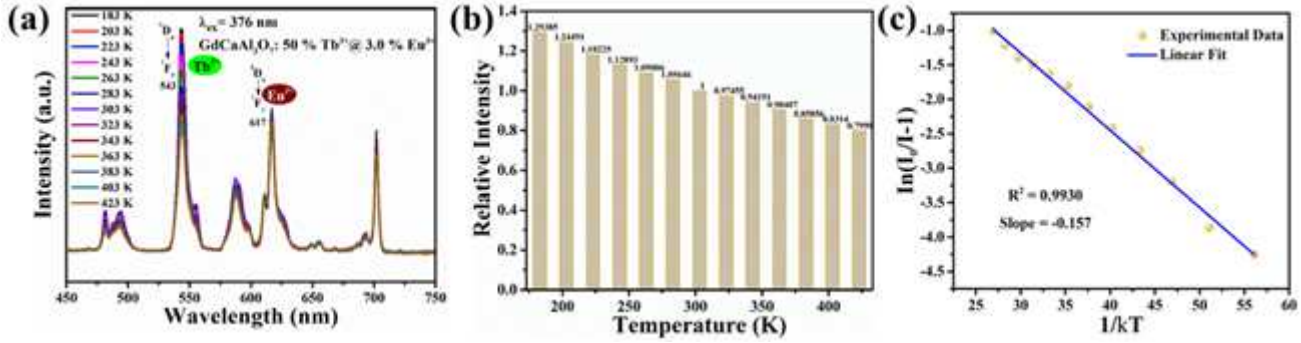


## Figure 10

(a) Temperature-dependent PL emission spectra, (b) normalized PL emission intensity and (c) plot of ln (I0/I-1) versus 1/kT in the GdCaAl3O7: 50% Tb3+@3.0% Eu3+.

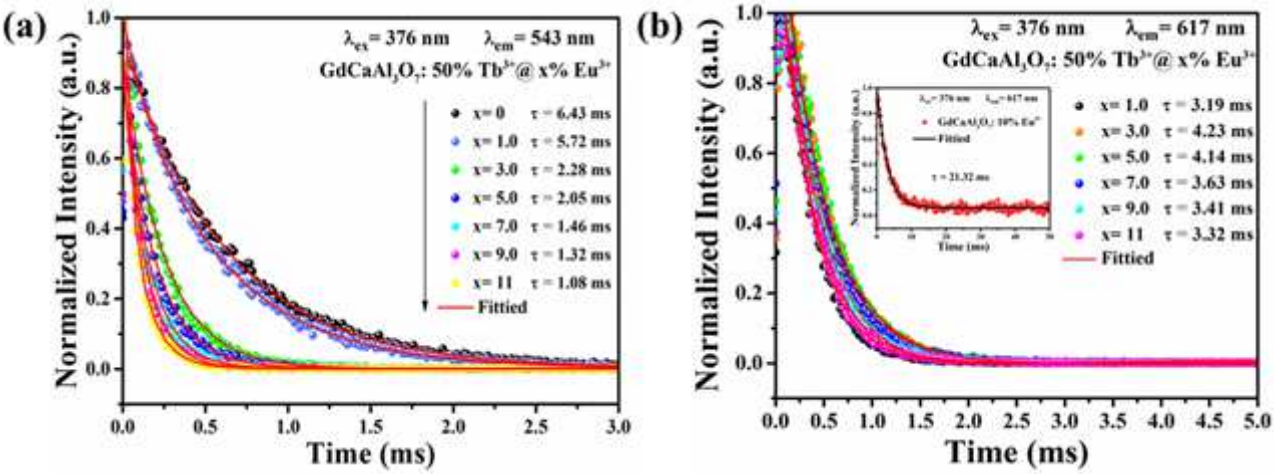


## Figure 11

Decay curves of the GdCaAl3O7: 50% Tb3+@x% Eu3+ (x= 1, 3, 5, 7, 9 and 11) monitored at (a) 543 nm emission and (b) 617 nm emission under the excitation of 376 nm.

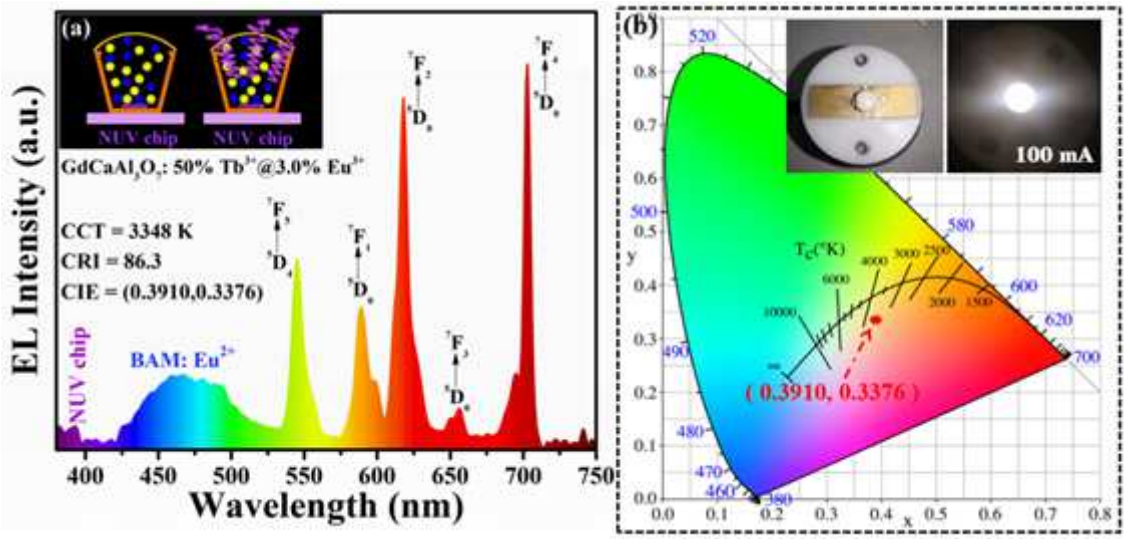


**Figure 12**

(a) EL emission spectra of the GdCaAl3O7: 50% Tb3+@3.0% Eu3+ by combining with BAM: Eu2+ on a NUV (~365 nm) chip. Inset: a schematic diagram for the preparation of white LED device. (b) CIE chromaticity diagram of prepared white-LEDs. Inset: the photographs of the packaged LED devices with injection current of 100 mA.

## Supplementary Files

This is a list of supplementary files associated with this preprint. Click to download.

- SupplementaryMaterials.docx